

# Mission Research Corporation

---

## Computational Support for Z-Machine

Thomas P. Hughes  
Robert E. Clark  
Bryan V. Oliver  
Richard A. St. John  
Mission Research Corporation

William A. Stygar  
Sandia National Laboratories

June 2002

Prepared for: SANDIA NATIONAL LABORATORIES  
P. O. Box 5800  
Albuquerque, NM 87185

Under Contract: Contract BD-4458

Prepared by: MISSION RESEARCH CORPORATION  
5001 Indian School Road, NE  
Albuquerque, NM 87110-3946  
(505) 768-7600

# Computational Support for Z-Machine

Thomas P. Hughes, Robert E. Clark, Bryan V. Oliver, Richard A. St. John

*Mission Research Corporation, Albuquerque, NM 87110*

William A. Stygar

*Sandia National Laboratories, Albuquerque, NM 87185*

June 26, 2002

## Acknowledgments

Several of the calculations in this report were performed on the DEC 8400 cluster and the Intel Teraflop at Sandia National Laboratories. The calculations for Figs. 3–6 were carried out by Chris Mostrom (MRC). The 3-D contour plots in Figs. 14–18 were made using the GMV plotting package (F. Ortega, LANL).

This work was supported by Sandia National Laboratories. Sandia is a multiprogram laboratory operated by Sandia Corporation, a Lockheed Martin Company, for the United States Department of Energy under Contract DE-AC04-94-AL85000.

# Contents

<b>1</b>	<b>Summary</b>	<b>1</b>
<b>2</b>	<b>Sheath Current in the Radial MITL's</b>	<b>3</b>
2.1	Fine Resolution Simulations . . . . .	4
2.2	Long Pulse Simulations . . . . .	10
<b>3</b>	<b>Long Pulse Simulations with Ion Emission</b>	<b>18</b>
<b>4</b>	<b>Neutral Desorption and Plasma Formation at Anode</b>	<b>21</b>
<b>5</b>	<b>Cathode Plasmas</b>	<b>27</b>
	<b>References</b>	<b>29</b>
<b>A</b>	<b>MITL Cathode Plasma Modeling</b>	
	<b>Thomas C. Genoni, Thomas P. Hughes, and Bryan V. Oliver</b>	<b>A-1</b>
A.1	Introduction . . . . .	A-1
A.2	Single-Fluid 1-D MHD Equations . . . . .	A-1
A.3	Plasma Conductivity Model . . . . .	A-2
A.4	Numerical Calculations . . . . .	A-3
A.5	Summary and Discussion . . . . .	A-5
A.6	Acknowledgements . . . . .	A-8
A.7	References . . . . .	A-9
<b>B</b>	<b>Magnetically Insulated Electron Flow On <math>Z</math> With Ions</b>	
	<b>Bryan V. Oliver, Robert E. Clark, and Thomas P. Hughes</b>	<b>B-1</b>
B.1	Introduction . . . . .	B-1
B.2	Model Equations . . . . .	B-2
B.3	Limiting Solutions . . . . .	B-3
B.4	Estimated sheath currents for $Z$ . . . . .	B-5
B.5	Conclusions . . . . .	B-7
B.6	Acknowledgements . . . . .	B-7
<b>C</b>	<b>Negative-Ion Current on the <math>Z</math> Machine</b>	
	<b>Richard St. John</b>	<b>C-1</b>
<b>D</b>	<b>Approximate Effect of Synchrotron Losses on a Magnetically Insulated Transmission Line</b>	
	<b>Richard St. John</b>	<b>D-1</b>

## List of Figures

1	Cutaway drawing of post-hole convolute on Z. Cathodes are shown in red, anodes in blue, posts in white. . . . .	1
2	Radial dependence of sheath-related quantities in MITL A of the Z machine. The sheath current and thickness are obtained by applying Eq. 1 locally at each radius. . . . .	4
3	Simulation geometries for two fine-resolution calculations in a radial MITL, using different terminations near 10 cm. . . . .	5
4	(a) Voltage (kV), and (b) current (amps) vs. time (ns) for finely resolved sheath simulations. Black traces are for simulation in Fig. 3(a), red traces are for simulation in Fig. 3(b). . . . .	6
5	Detail of calculation in Fig. 3(b), overlaying the numerical grid on a particle plot near the outer radius of the MITL. Dimensions are in cm. . . . .	8
6	Current (A) vs. time (ns) at radii of 49.5, 35, 20, and 10 cm in the MITL for (a) Fig. 3(a) and (b) Fig. 3(b). Averages are given in Table 1. . . . .	9
7	Schematic of a forward wave front in a MITL. Transverse electron currents can be divided into two categories; stationary currents due to geometry changes (left side of the figure), and moving currents due to time-dependent behavior (right side of the figure). (This figure and caption are from Ref. 8.) . . . . .	10
8	Snapshots of the electron sheath at a sequence of radial positions. A detail near 27 cm is shown in (h). All dimensions are in cm. . . . .	11
9	Schematic of sheath liftoff in a Z-like radial line, to preserve flow impedance. Compare simulation results in Figs. 8 and 10. . . . .	12
10	Geometry of full-pulse simulations of MITL A. . . . .	12
11	Forward-going voltage applied at the outer boundary in Fig. 10. . . . .	14
12	Current, voltage and impedance waveforms at 50 cm for the simulation in Fig. 10. . . . .	15
13	Load current (MA) and radius (mm) for the simulation in Fig. 10. . . . .	16
14	Color-coded plot of anode temperature rise (K) due to electron impact, for simulation in Fig. 10. . . . .	16

15	Sheath current vs. time at different radial positions in the MITL. . . . .	17
16	Snapshot of long-pulse simulation with ion (proton) emission from the anode.	18
17	Effect of anode ion emission in radial MITL. Plot (a) shows total current vs. time at different radial positions in the MITL, and (b) shows peak current as a function of radial position. . . . .	19
18	Color-coded plots of anode heating due to electron impact in 3-D calculation of convolute for two different temperature ranges: (a) 0–200 K and (b), (c) 0–1000 K. In (a) and (b) the outer radius (left) is at 30 cm, and the inner radius is at 4.4 cm from the central axis (larger than the actual inner radius on Z). Plot (c) is a close-up of the convolute from a different angle. The axes on the bottom are to show the scale (in cm) only. . . . .	22
19	(a) Current loss and (b) electron sheath current as functions of time going through the convolute for simulation in Fig. 18. . . . .	23
20	Snapshots of particle positions (projected onto the $\theta = 0$ plane) from a 3-D simulation of convolute with neutral desorption /ionization. . . . .	25
21	Schematic for calculation of forces on cathode plasma. . . . .	28
A-1	The anomalous collisionality (a) and conductivity (b) as a function of the density $n$ (in $\text{cm}^{-3}$ ) and magnetic field $B$ (in gauss). The collisionality is normalized by the Coulomb collision frequency $\nu_{ei}$ and the conductivity by the Spitzer value $\sigma_0 = (ne^2/m\nu_{ei})$ . A plasma temperature $T = 10$ eV is assumed. . . . .	A-4
A-2	Evolution of density profile of 1 eV proton plasma expanding against ramped magnetic field (peak 5 tesla). . . . .	A-6
A-3	Same as Fig. A-2 for peak magnetic field 10 tesla. . . . .	A-6
A-4	Expansion of proton plasma at $t = 100$ ns with and without ramped magnetic field (peak 10 tesla). . . . .	A-7
A-5	Same as Fig. A-3 for 1 eV $\text{C}^{+3}$ plasma. . . . .	A-7
A-6	Same as Fig. A-4 for 1 eV $\text{C}^{+3}$ plasma. . . . .	A-8
B-1	Illustration of the cartesian equivalent radial feed MITL. . . . .	B-2
B-2	Normalized MITL anode current as a function of $\gamma_s$ with and without ions. The voltage $V = 2$ MV. . . . .	B-5

B-3 Anode current vs.  $\gamma_s$  with and without ions for a) high impedance operation ( $I_a = 1$  MA,  $V = 1.3$  MV,  $g = 20$ ) and b) low impedance operation ( $I_a = 5.4$  MA,  $V = 2.1$  MV,  $g = 10$ ). . . . . B-6

# 1 Summary

An important issue in designing a higher-power version of the Z machine at Sandia National Laboratories (SNL) is current loss in the vacuum section, which consists of four radial transmission lines and a convolute (current-adder) (Fig. 1). There is evidence from experiments on Z that 1–2 MA of current out of about 20 MA are lost in the vacuum section before reaching the wire-array load [1]. Calculations using particle-in-cell codes have shown much less current loss [2,3]. The current loss seen in the numerical calculations occurs in the region of the convolute, and is associated with the magnetic nulls which are intrinsic to the current crossovers in the convolute [2,3]. There are a number of mechanisms which could enhance the loss-current: (a) launching of vacuum electron flow in the low-impedance, large-radius region of the MITL's where the sheath current is much larger than at smaller radius, (b) ion emission from the anode and (c) gap closure due to cathode-plasma expansion. In Sec. 2 we examine launched electrons. Sections 3 and 4 discuss anode ion and plasma formation, respectively. Section 5 has rough estimates for cathode plasma dynamics. A numerical treatment of the cathode plasma is given in Appendix A. Anode ion effects on the cathode electron sheath are treated in greater detail in Appendix B. Data from earlier experiments to measure negative ion current from the cathode are reviewed in Appendix C.

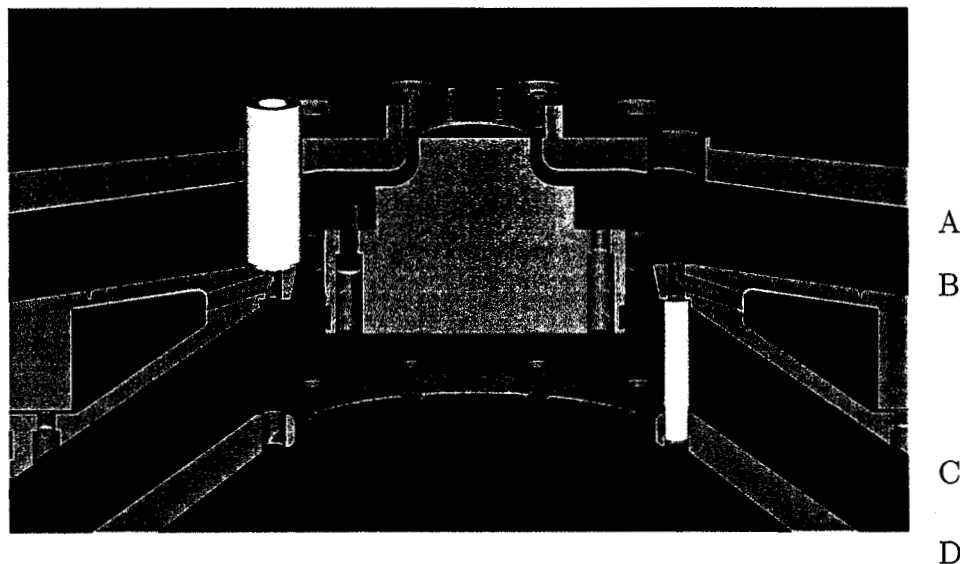


Figure 1: Cutaway drawing of post-hole convolute on Z. Cathodes are shown in red, anodes in blue, posts in white.

The main conclusion from this work are:

1. In the region between the insulator stack and a radius of about 20 cm, over which the radial-line vacuum impedance increases slowly, excess electron sheath current is mostly retrapped to the cathode, and the sheath current decreases significantly as a result. Between a radius of 20 cm and the convolute, where the radial-line vacuum impedance increases more sharply, there is significant "launching" of sheath current. The sheath behavior in this region is qualitatively similar to Cliff Mendel's "conservation of flow-impedance" model, but in the simulations, the sheath is unstable and breaks up into vortices.
2. A 3-D simulation of the upper two MITL's shows current loss on the order of 100 kA at the peak of the current waveform. Estimating 200 kA loss for the full 4-MITL convolute yields a significant discrepancy with the 1-2 MA current loss inferred from the experimental data.
3. Ion emission, either as negative ions from the cathode, or as positive ions from the anode, can account for several MA of current loss if space charge limited flow is permitted out to a radius of order 50 cm. If space charge limited ion emission is confined to the region of the convolute, the ion loss current is of order 200 kA.
4. A convolute calculation with adsorbed neutral monolayers on the anode shows avalanche generation of plasma near the hottest part of the anode. However, it appears that the plasma is generated too late in the pulse to effect the peak current.
5. A one-dimensional model of cathode plasma motion shows expansion at roughly the free-expansion rate, despite the presence of a strong transverse magnetic field. This is because diffusion of the magnetic field into the cathode plasma is sufficiently rapid that most of the cathode current is carried by the conductor, rather than on the surface of the plasma.

## 2 Sheath Current in the Radial MITL's

Analytic treatments of magnetically insulated electron sheaths have been given for equilibrium, one-dimensional cases [4–6]. A simple expression based on force-balance, due to Mendel [5], gives the equilibrium electron sheath current at radius  $r$  in a radial transmission line as:

$$I_s(r) \approx \frac{V^2}{2I_a Z_v^2} = 1.4 \times 10^{-4} \frac{V^2 r^2}{I_a a^2}, \quad \text{where}$$

$$V = Z_f (I_a^2 - I_c^2)^{1/2} \approx Z_v (I_a^2 - I_c^2)^{1/2} \quad (1)$$

where  $V$  is the A-K voltage (volts),  $I_a, I_c$  are the currents flowing in the anode and cathode conductors (amps), respectively,  $a(r)$  is the AK gap,  $Z_v$  is the MITL characteristic impedance and  $Z_f$  is the “flow impedance”, defined as the characteristic impedance of the line between the equilibrium centroid position of the electron sheath and the anode conductor [5]. Creedon’s treatment [4] gives an equivalent expression in the appropriate limit. Creedon shows that the expressions for a uniform parallel-plate transmission line also apply to a radial transmission line with constant impedance, i.e., where the anode-cathode gap is proportional to the radius. In this case, the equilibrium sheath current is independent of the radius.

In the Z machine, the anode-cathode gap is almost proportional to radius down to a radius of 50 cm, as shown in Fig. 2. The gap then decreases at a slower rate to a radius of 20 cm, at which point the gap remains constant at 1 cm down to the edge of the convolute at about  $r = 10$  cm. An important question is how the sheath current changes as the impedance increases near the convolute. According to Eq. 1, the sheath current decreases as  $1/r^2$  in the constant-gap section between 20 cm and 10 cm. Thus electron sheath current flowing in from larger radius must either be retrapped on the cathode, or somehow “launched” off the cathode surface. We have carried out 2-D simulations of a single MITL using LSP [7] to look at this issue. We find that Eq. 1 is approximately true at each radial position down to a radius about 20 cm, where the AK gap becomes constant (see Fig. 2). From this radius inward, the simulated sheath current exceeds the Eq. 1 current. However, the sheath current is significantly smaller than that in the  $2 \Omega$  section at larger radius.

Below, we describe two sets of calculations which illustrate this behavior: (a) fine resolution simulations where the electron sheath on the cathode is resolved, but the calculation runs only for a few nanoseconds and (b) more coarsely resolved simulations where the electron sheath is not resolved, but the calculation is run for a full Z-like pulse.

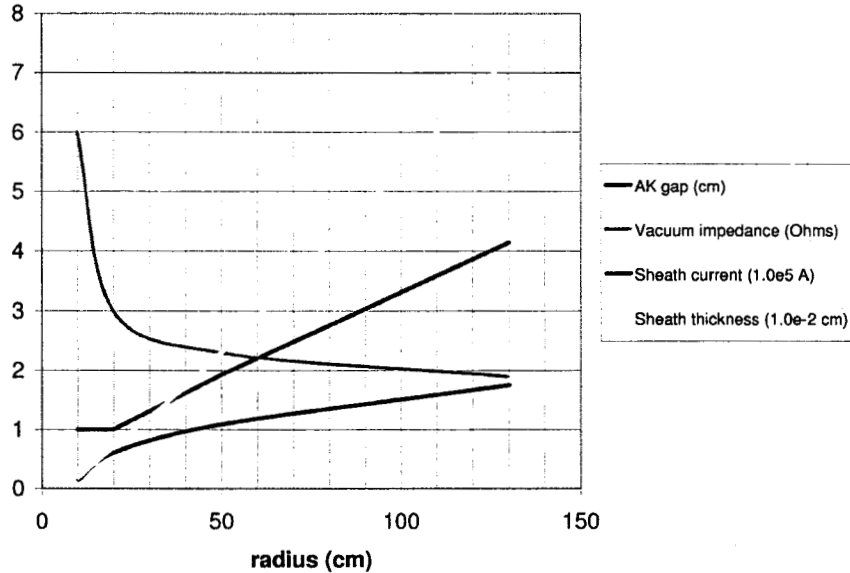


Figure 2: Radial dependence of sheath-related quantities in MITL A of the Z machine. The sheath current and thickness are obtained by applying Eq. 1 locally at each radius.

## 2.1 Fine Resolution Simulations

For the fine resolution cases, we simulate a region from about 10 to 50 cm in radius. To obtain a practical running time, we use a reduced anode-cathode gap, and scale the voltage accordingly. In this way, the electric and magnetic fields at the cathode surface are the same as those for the full AK gap, but the number of cells needed is much reduced. Following a suggestion by Tim Pointon, two different boundary conditions at the inner radius were used: a simple outgoing-wave radial boundary, and a stepped boundary intended to capture some of the effects of the post-hole geometry (see Fig. 3). Near the cathode surface, the resolution is 0.01 cm in the radial ( $r$ ) direction, and 0.0025 cm (25 microns) in the transverse ( $z$ ) direction. The simulations are run to steady-state vacuum conditions of 0.2 MV (scaled from 2 MV) and 4 MA before cathode emission is allowed (cf. Fig. 12). When emission is turned on, the calculation is continued for several nanoseconds. Voltage and current traces are shown in Fig. 4. At 0.2 MV, 4 MA, the local, equilibrium electron sheath thickness is given roughly by the following equation (based on Eq. 1)

$$d_s \simeq \frac{142Vr^2}{I_a^2 a} \quad (2)$$

where  $V$  is in volts,  $I_a$  is in amps, and  $d_s$ ,  $r$ ,  $a$  are in centimeters. At a radius of 50 cm, this gives a thickness of 0.023 cm, which is well-resolved by the mesh (cf. Fig. 5), while at 10 cm, it gives a thickness of 0.002 cm, which is of order the cell size and so is not resolved.

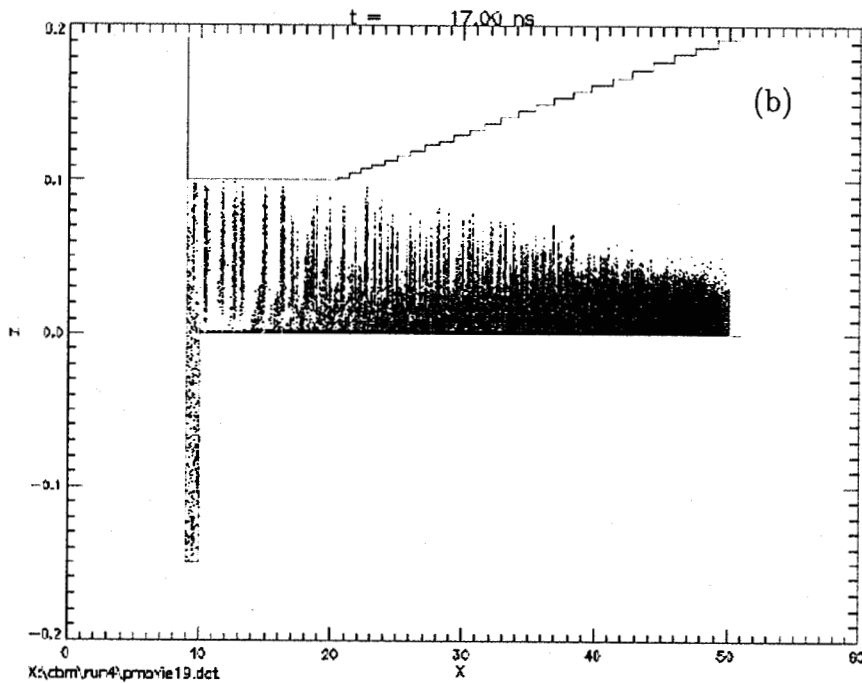
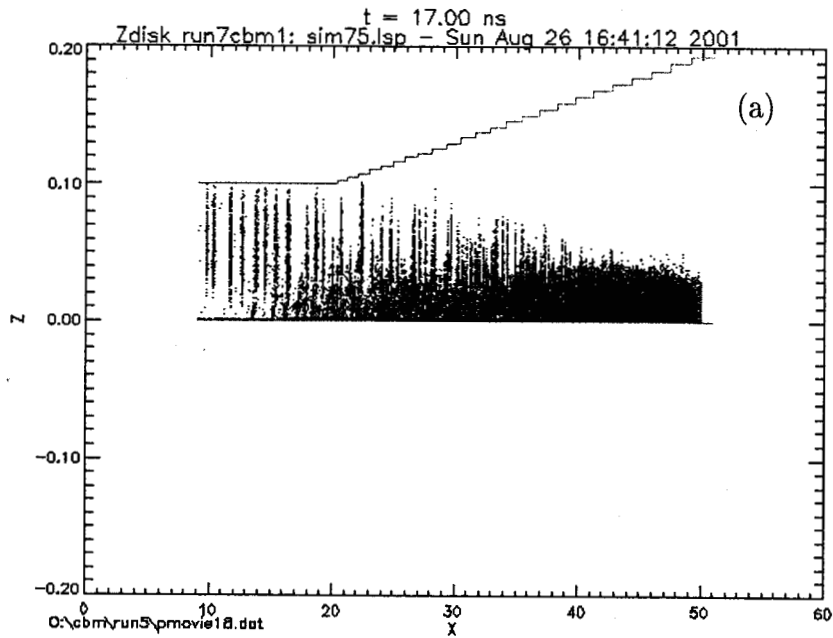
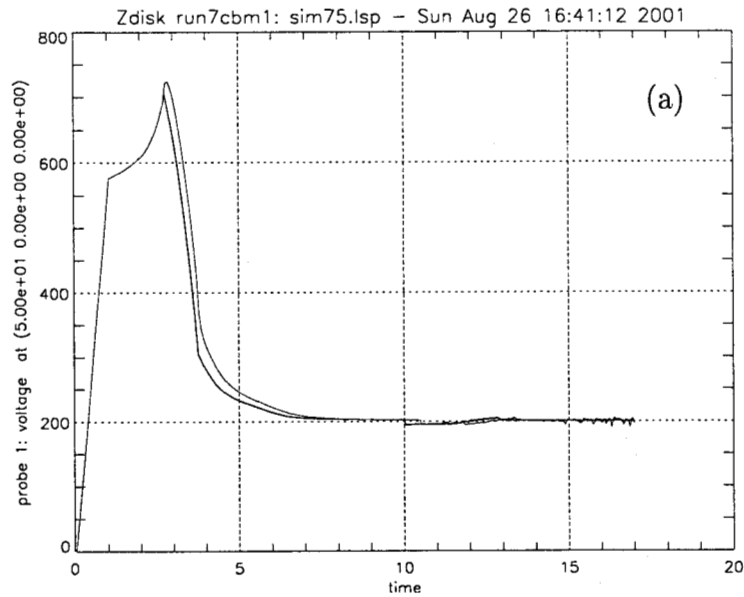
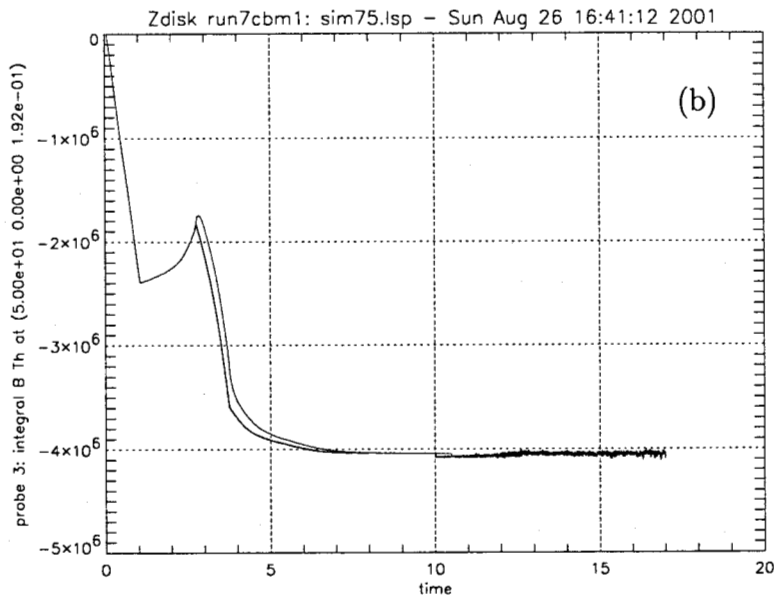


Figure 3: Simulation geometries for two fine-resolution calculations in a radial MITL, using different terminations near 10 cm.



PLOT LABELS  
 probe 1: voltage at (5.00e+01 0.00e+00 0.00e+00)  
 probe 1: voltage at (5.00e+01 0.00e+00 0.00e+00) [Zdisk run7cbm1: sim74.lsp - Sat Aug 18 15:47:53 2001  
 File = O:\cbm\run5\history.dat : Oct 04 17:22:17 2001



PLOT LABELS  
 probe 3: integral B Th at (5.00e+01 0.00e+00 1.92e-01)  
 probe 3: integral B Th at (5.00e+01 0.00e+00 1.92e-01) [Zdisk run7cbm1: sim74.lsp - Sat Aug 18 15:47:53 :  
 File = O:\cbm\run5\history.dat : Oct 04 17:24:05 2001

Figure 4: (a) Voltage (kV), and (b) current (amps) vs. time (ns) for finely resolved sheath simulations. Black traces are for simulation in Fig. 3(a), red traces are for simulation in Fig. 3(b).

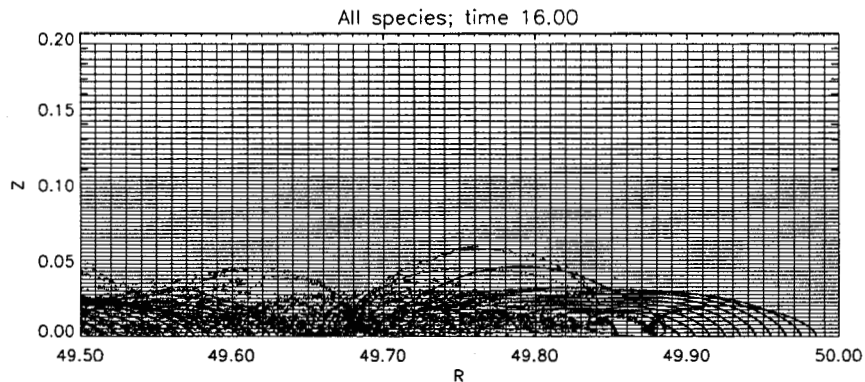
We compare the sheath currents at four radii in Table 1. We see that there is reasonably good agreement with Eq. 1 down to 20 cm. At 10 cm, however, the sheath current is about 2.5 times larger than the analytic result, but still about 3 times smaller than the current at 50 cm. It appears that there is substantial retrapping of the sheath current in the region between 50 cm and 20 cm as the impedance slowly increases from  $2.3 \Omega$  to  $3 \Omega$ . Between 20 and 10 cm the impedance increases more rapidly from  $3 \Omega$  to  $6 \Omega$  (see Fig. 2), and a larger amount of the sheath current is “launched” in the form of electron vortices instead of being retrapped. The averages in Table 1 disguise the dynamics at small radius, where the electron sheath current is made up of a local component roughly obeying Eq. 1 with the local  $Z_v$ , and a periodic component due to launched flow from upstream. This is shown in Fig. 6.

The considerable amount of retrapping observed, particularly where the impedance is changing slowly with radius, means that the results differ from the picture described by Mendel et al. in Ref. [8] (Fig. 7), based on a simple thin-layer model for the vacuum flow. According to this picture, if the vacuum impedance of a MITL increases along the direction of power flow, the electron layer moves towards the anode in order to remain force-balanced. This also preserves the flow impedance, defined as the vacuum impedance between the electron layer and the anode. Thus in this model no retrapping occurs. In the simulations, however, as the electron layer tries to lift off the cathode it becomes unstable, leading to the formation of vortices (Fig. 8). The instability may be providing the mechanism for returning electrons to the cathode. Thus, Eq. 1 can be satisfied while allowing the flow impedance,  $Z_f$ , to increase rather than remain constant.

The thin-layer model [8] is, however, useful for qualitatively understanding the motion of the electron vortices launched in the constant-gap section of the MITL. The model makes different equilibrium predictions for the full AK gap and the scaled AK gap. To see why, it is best to think of the scaled simulations in terms of placing the electron sheath close to anode, as opposed to moving the anode close to the cathode conductor. This is because, in order to stay force-balanced, the average sheath position moves to preserve the upstream impedance. In a radial transmission line, this means that the distance between the electron layer and the anode must scale linearly with the radius. So, for example, to preserve a flow impedance of  $2.3 \Omega$  (the value at large radius) at a radius of 10 cm (where the vacuum impedance is  $6 \Omega$ ), the electron layer would need to move about 0.66 cm off the cathode surface for the full AK gap, as illustrated in Fig. 9. For the scaled simulations, however, the upstream impedance is only  $0.23 \Omega$  and the electron sheath centroid only has to move 0.066 cm off the cathode to keep this impedance at 10 cm radius. In the simulations, the trajectories of the launched

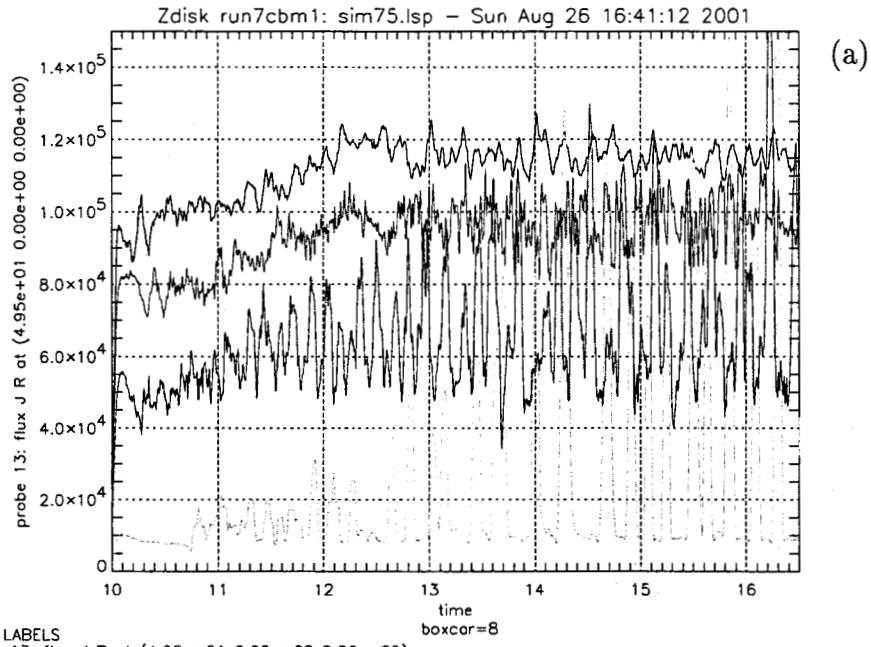
Table 1: Comparison of sheath current in finely-resolved “MITL A” simulations vs. equilibrium analytic value. Voltage = 0.2 MV (scaled from 2 MV), current = 4 MA. Run 5 is for a simple radial termination. Run 4 is for an axial termination.

Radius (cm)	Gap (cm)	$Z_v(\Omega)$	Current (kA)		
			Run 5	Run 4	Eq. 1
49.5	1.93	2.3	115	115	108
35	1.45	2.5	97	96	92
20	1	3	74	74	60
10	1	6	38	35	14

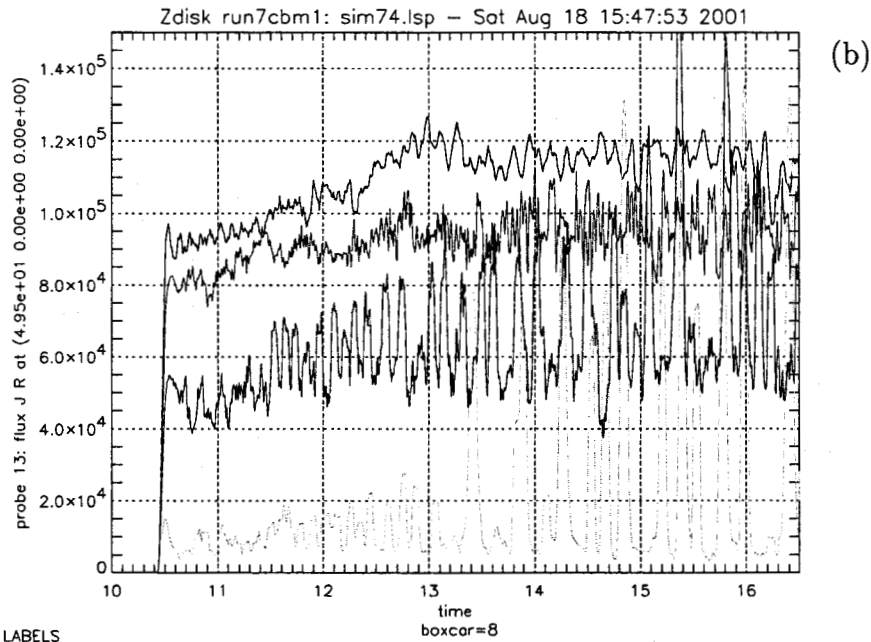


File = O:\cbm\run4\p219750.dot : Oct 03 19:17:30 2001

Figure 5: Detail of calculation in Fig. 3(b), overlaying the numerical grid on a particle plot near the outer radius of the MITL. Dimensions are in cm.



File = 0:\cbm\run5\history.dat : Oct 04 17:34:43 2001



File = 0:\cbm\run4\history.dat : Oct 04 17:44:19 2001

Figure 6: Current (A) vs. time (ns) at radii of 49.5, 35, 20, and 10 cm in the MITL for (a) Fig. 3(a) and (b) Fig. 3(b). Averages are given in Table 1.

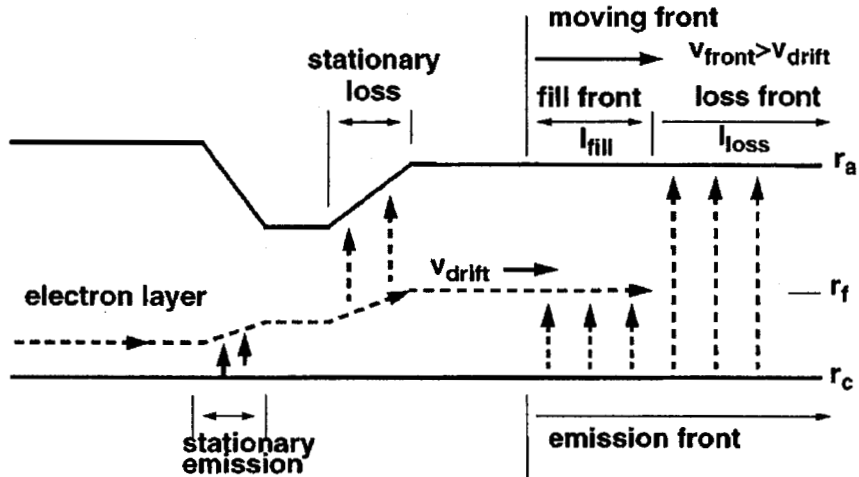


Figure 7: Schematic of a forward wave front in a MITL. Transverse electron currents can be divided into two categories; stationary currents due to geometry changes (left side of the figure), and moving currents due to time-dependent behavior (right side of the figure). (This figure and caption are from Ref. 8.)

vortices are in rough agreement with this estimate. In the following section, we show results for the full AK gap, but with cruder resolution than for the above scaled simulations.

## 2.2 Long Pulse Simulations

To examine electron flow in the MITL's for a full Z pulse (about 130 ns), we use a coarser mesh. One of the motivations for these calculations is to measure anode heating due to electron impact, which primarily occurs early in the pulse when magnetic insulation is being established. The geometry is shown in Fig. 10.

The forward-going voltage applied at the outer boundary at 60 cm is shown in Fig. 11. The coaxial transmission line at the upper left of Fig. 10 is terminated by a simple imploding-liner model (similar to that in Screamer). Since we are only simulating one MITL, the current into the liner is multiplied by a factor of 4 to roughly simulate the total current. The current, voltage and impedance waveforms at 50 cm are shown in Fig. 12. The load current and radius are shown in Fig. 13. A color-coded plot of the anode temperature shown in Fig. 14. The temperature rise is only on the order of 100K, insufficient to cause any significant increase in the desorption of neutrals. The sheath currents at different radii are shown in Fig. 15. The peak at early time is due to the "loss front" during the time between exceeding the emission threshold and establishment of magnetic insulation. For this calculation we have

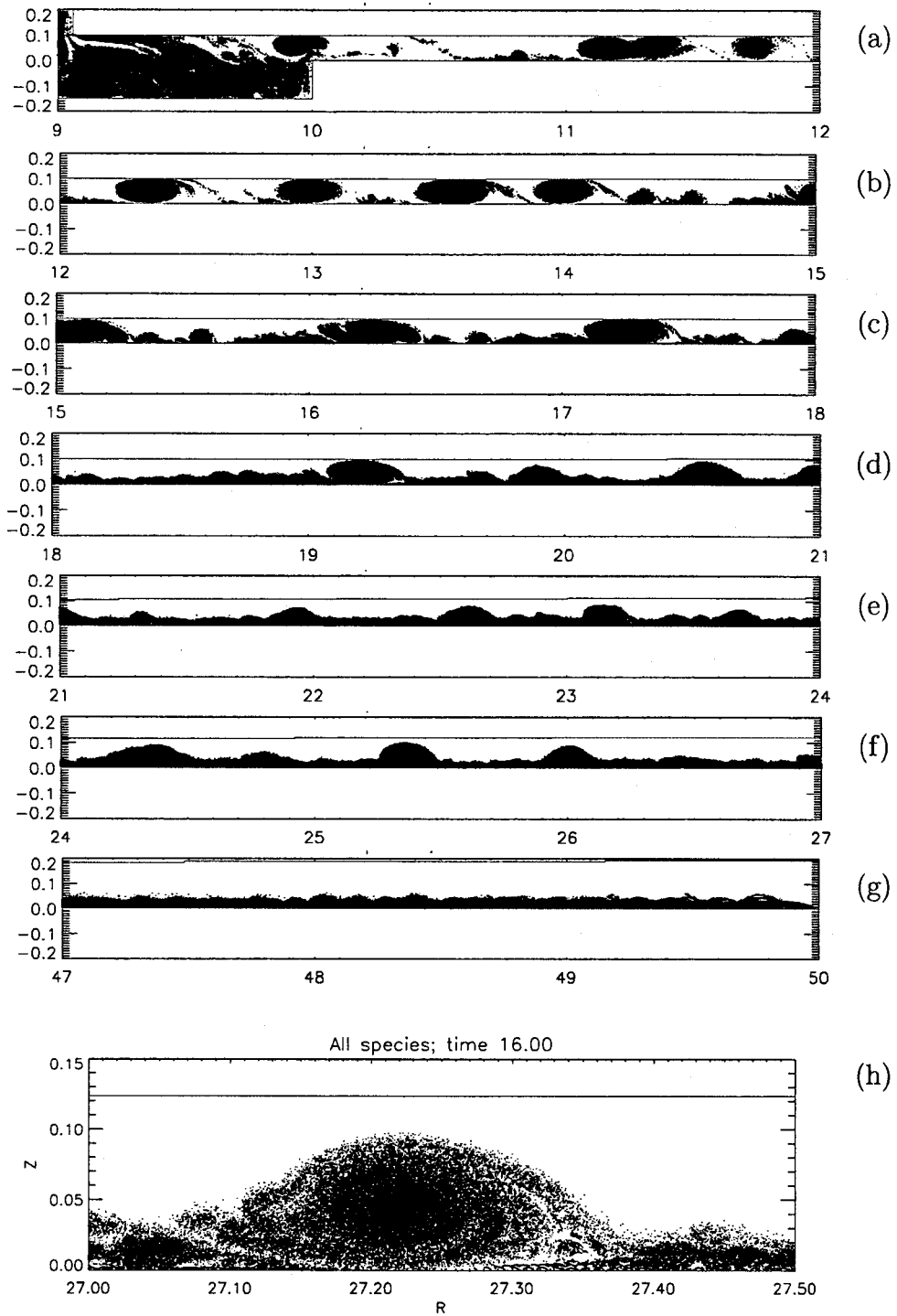


Figure 8: Snapshots of the electron sheath at a sequence of radial positions. A detail near 27 cm is shown in (h). All dimensions are in cm.

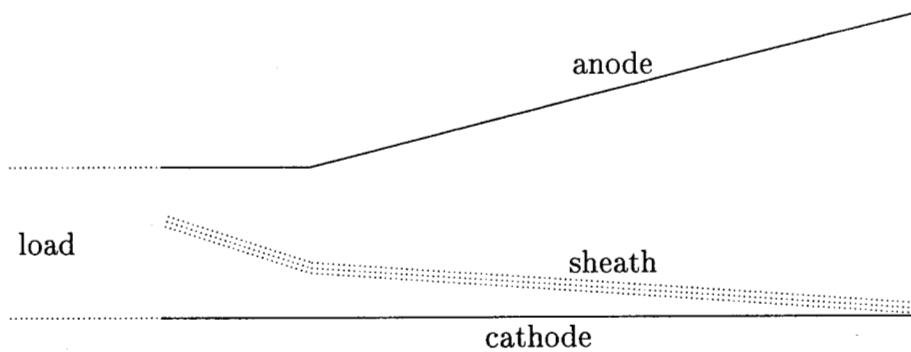


Figure 9: Schematic of sheath liftoff in a Z-like radial line, to preserve flow impedance. Compare simulation results in Figs. 8 and 10.

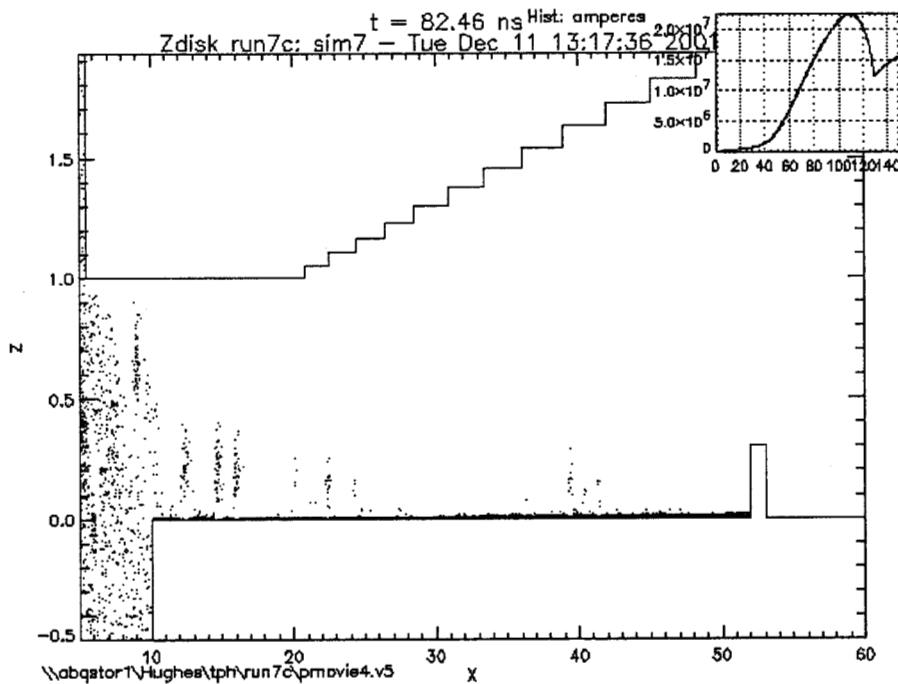


Figure 10: Geometry of full-pulse simulations of MITL A.

assumed a threshold of 250 kV/cm. The peak at late time is due to the voltage spike as the imploding liner reaches minimum radius (Fig. 13). When magnetic insulation is established, the electron sheath shrinks to a size much smaller than the transverse cell size, so we cannot expect to accurately model the sheath dynamics. However, the sheath current in the simulation shows roughly the same trend as the fine-resolution simulations described above. The sheath current at peak total current (about 110 ns in Fig. 15) are compared to Eq. 1 in Table 2. Note that the electron vortices launched in the simulation move out roughly half way into the gap (see Fig. 10), similar to those in the simulation with the scaled AK gap (see discussion at the end of Sec. 2.1).

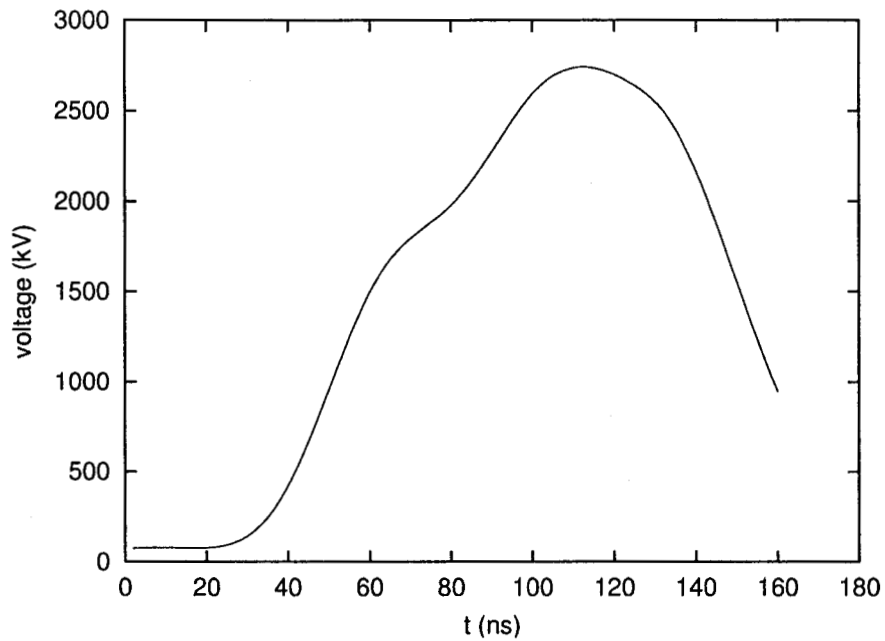


Figure 11: Forward-going voltage applied at the outer boundary in Fig. 10.

Table 2: Sheath currents at peak total current for simulation in Fig. 10.

Radius (cm)	Gap (cm)	$Z_v(\Omega)$	Current (kA)	
			Simulation	Eq. 1
50	1.93	2.3	75	149
35	1.45	2.5	75	127
20	1	3	53	84
10	1	6	40	20

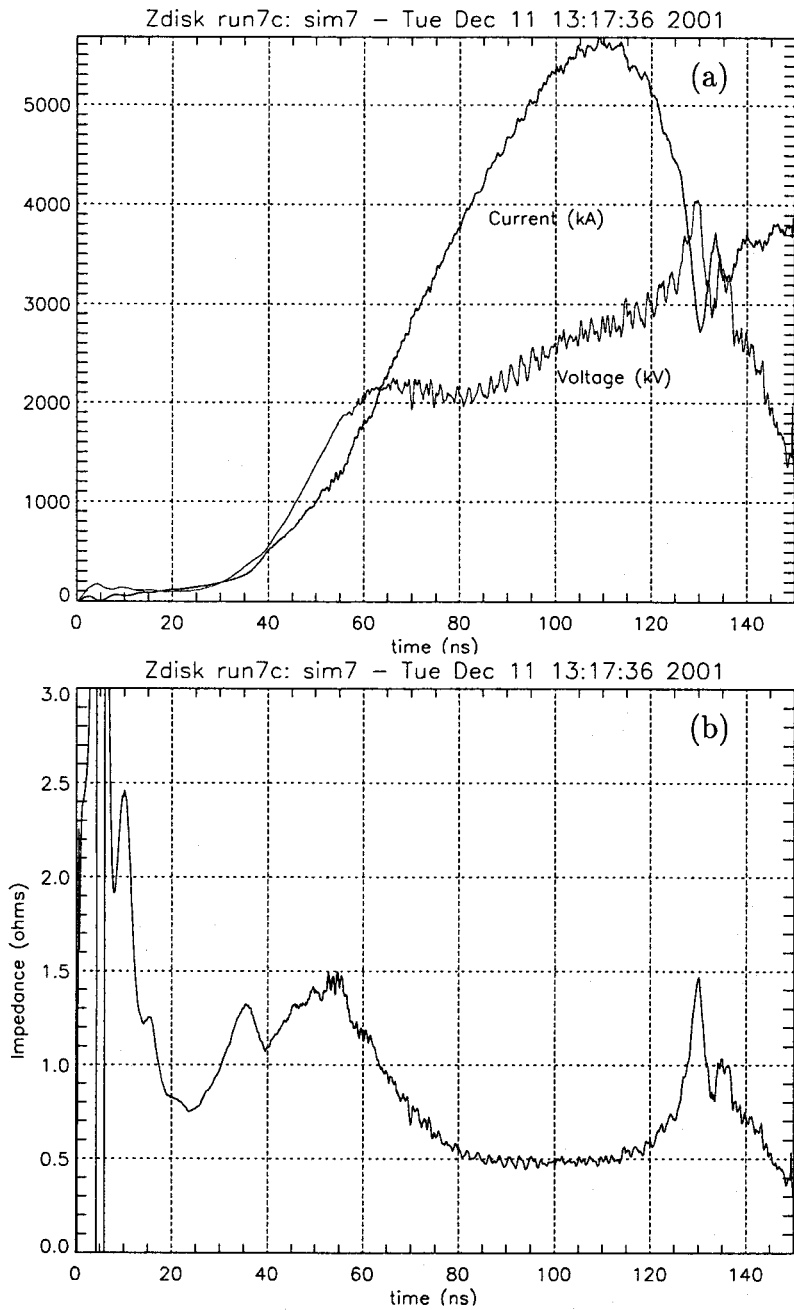


Figure 12: Current, voltage and impedance waveforms at 50 cm for the simulation in Fig. 10.

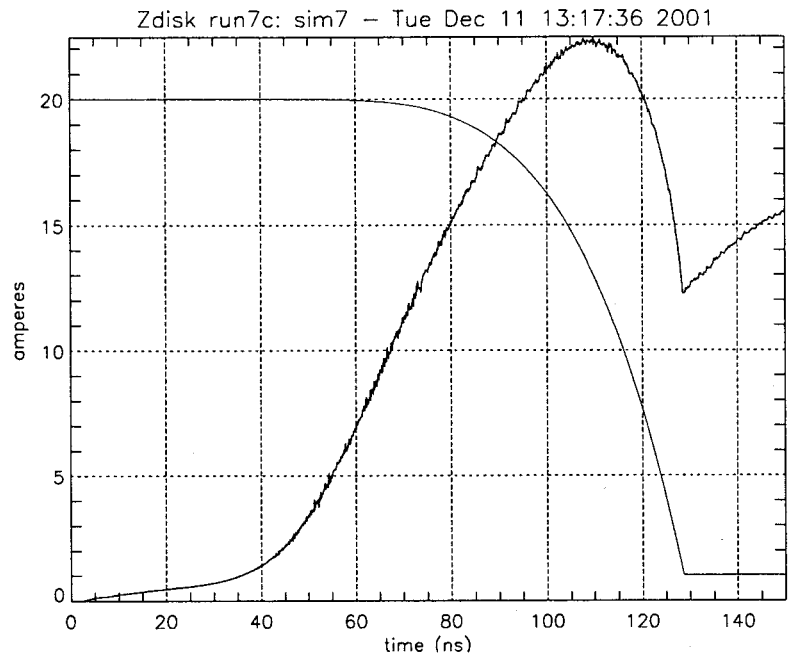


Figure 13: Load current (MA) and radius (mm) for the simulation in Fig. 10.

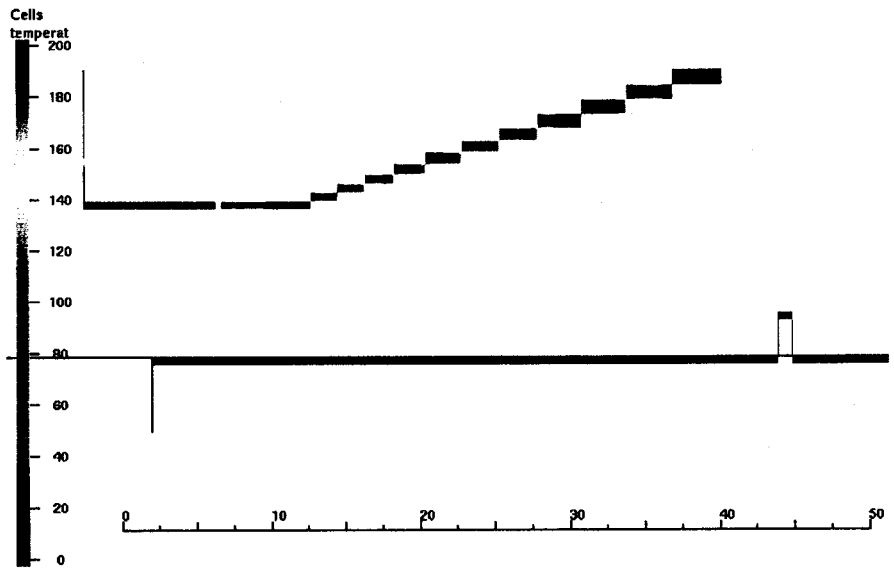


Figure 14: Color-coded plot of anode temperature rise (K) due to electron impact, for simulation in Fig. 10.

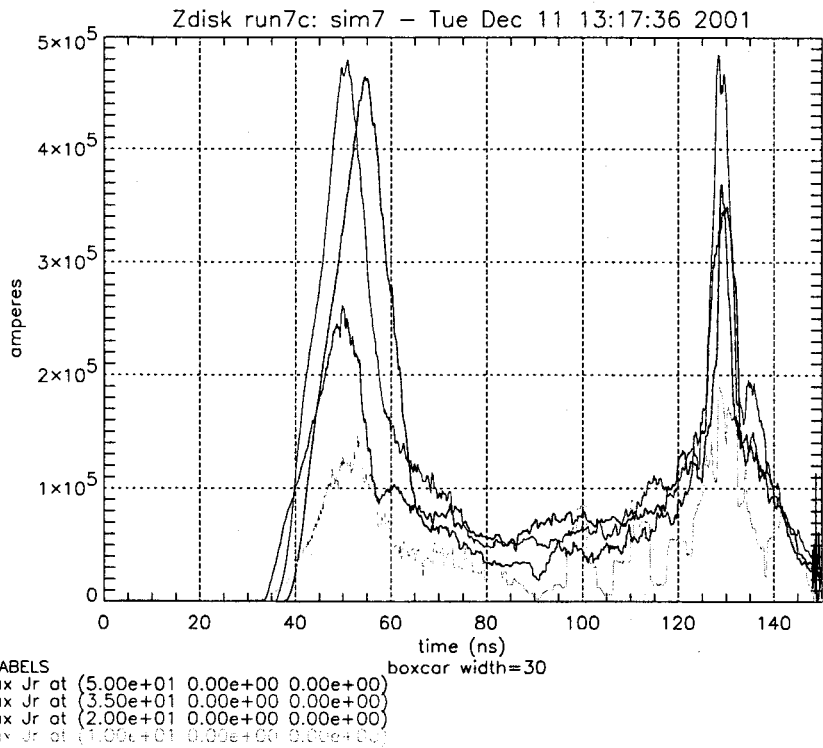


Figure 15: Sheath current vs. time at different radial positions in the MITL.

### 3 Long Pulse Simulations with Ion Emission

One possible mechanism for current loss in the MITL's is ion emission: positive ion emission from the anode, and/or negative ion emission from the cathode (see Appendix C). The vacuum electrodes in Z have a large surface area so that a small ion current density could produce substantial losses. To estimate this, we allowed spacecharge-limited anode emission of protons from a long-pulse simulation of the type described in the previous section. A snapshot from this calculation is shown in Fig. 16. Total current waveforms at different radii are shown in Fig. 17. We see that the ion loss current is over 3 MA between 50 and 10 cm, more than enough to explain the observed losses (of order 1–2 MA). However, it is difficult to justify treating the anode as a spacecharge-limited emitter of ions. The results in section 2.2 show that heating of the anode due to electron impact is only of order 100 K. UV radiation from the cathode plasma is probably too weak to produce anode ions, though we have not investigated this in any detail. Diode experiments at NRL by Hinshelwood [9], which used laser interferometry to observe both the anode and cathode surfaces, did not show any evidence of anode plasma formation, in spite of direct heating and bombardment by electrons, in addition to UV radiation.

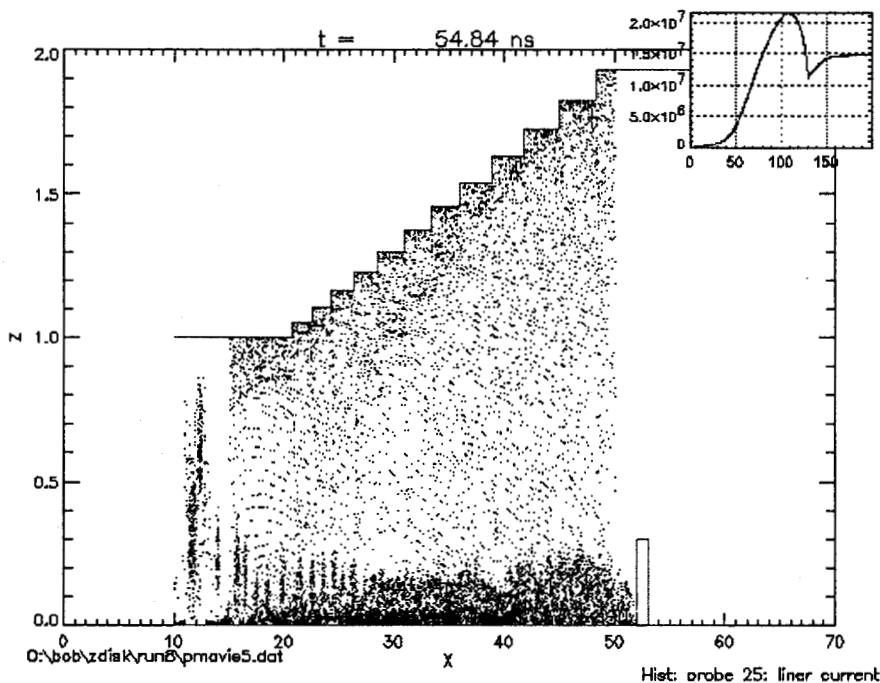
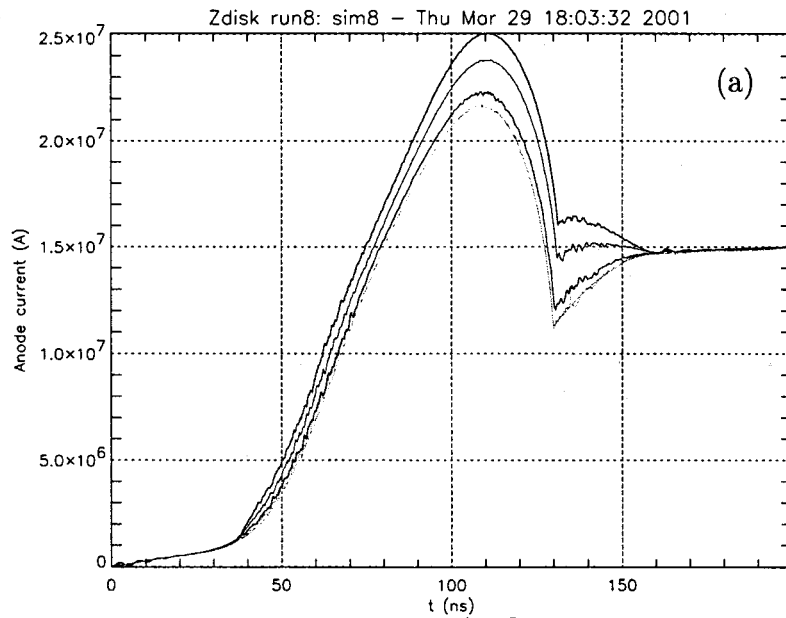


Figure 16: Snapshot of long-pulse simulation with ion (proton) emission from the anode.



PLOT LABELS  
 boxcar width=5  
 probe 3: integral B Th at (5.00e+01 0.00e+00 1.92e+00) [Zdisk run8: sim8 - Thu Mar 29 18:03:32 2001]  
 probe 6: integral B Th at (3.50e+01 0.00e+00 1.45e+00) [Zdisk run8: sim8 - Thu Mar 29 18:03:32 2001]  
 probe 9: integral B Th at (2.00e+01 0.00e+00 9.90e-01) [Zdisk run8: sim8 - Thu Mar 29 18:03:32 2001]  
 probe 12: integral B Th at (1.00e+01 0.00e+00 5.00e-01) [Zdisk run8: sim8 - Thu Mar 29 18:03:32 2001]  
 probe 25: linear current [Zdisk run8: sim8 - Thu Mar 29 18:03:32 2001]

File = O:\bob\zdisk\run8\history.dat : Nov 16 18:32:36 2001

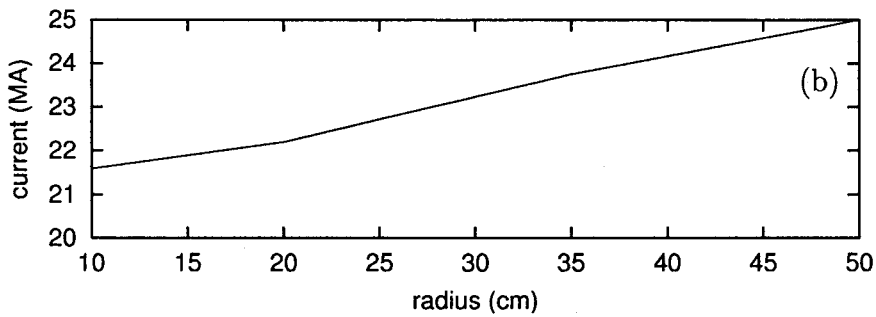


Figure 17: Effect of anode ion emission in radial MITL. Plot (a) shows total current vs. time at different radial positions in the MITL, and (b) shows peak current as a function of radial position.

Allowing spacecharge-limited emission of negative ions from the cathode would produce roughly the same loss current. Experiments at SNL have shown the presence of negative ions, but there is considerable uncertainty about the current density [10]. This is discussed in Appendix C. We believe that it would be worthwhile to carry out some experiments looking for positive and negative ions, in order to put a bound on their contribution to current.

We have made a rough estimate of energy loss due to synchrotron radiation from the electron sheath (Appendix D). This is found to have a negligible effect on the electron dynamics; it may, however, be of interest for diagnostic purposes.

## 4 Neutral Desorption and Plasma Formation at Anode

Previous 3-D simulations of the current-carrying convolute in Z have shown regions of significant electron-impact heating which correspond to post-shot damage patterns on the anode hardware [2]. These calculations went out to a radius of 14 cm where the line impedance is about  $4.3 \Omega$  (vs.  $2 \Omega$  at larger radius), and included only cathode-emitted electrons. The calculations reported here extend the simulation boundary to 30 cm ( $2.6 \Omega$  line impedance) in order to include more of the impedance transition. The results in Secs. 2.1 and 2.2 indicate that there is little “launched” current beyond this radius, i.e. the sheath current is determined by applying Eq. 1 locally. We have included the effect of thermal desorption of neutrals from the anode surface, and the subsequent ionization of these neutrals. The motivation is to see if this effect can contribute significant ion loss current. Spacecharge-limited ion emission provides an upper bound on the amount of loss current due to creation of ions on anode surfaces, and if this emission is confined to the region of the convolute (the region inside a radius of 11 cm), it would only amount to about 200 kA. We are more interested in the possibility of generating hot, relatively dense plasma due to avalanche ionization in a desorbed neutral layer. This could result in AK gap narrowing or closure, leading to significantly more current loss than just spacecharge-limited emission from the anode surface.

The geometry of the calculation is shown in Fig. 18. The 3-D calculation is terminated at the inner radius the same way as the 2-D calculation in Fig. 10, i.e., with an imploding-liner model. To cut the calculation time, only the upper two MITL’s are gridded. The lower two MITL’s are modeled as an effective transmission line which attaches to the coaxial opening at the bottom of Fig. 18. To further reduce calculation time, we have cut 20 ns from the beginning of the forward-going pulse applied at the three inlets. This results in a delay in the onset of magnetic insulation, but the temperature rise of the outer anode is still only on the order of 100K or less. The current loss in going through the convolute is shown in Fig. 19(a). The current loss is defined as the sum of the currents in the upper two MITL’s and that entering from the lower two MITL’s minus the current at the inner radius in Fig. 18. Since only the upper two MITL’s are simulated, we should approximately double the values shown in this figure. At the time of peak current (90 ns in Fig. 19), the loss current is only on the order of 100 kA (200 kA if the lower two MITL’s are assumed to have similar losses), significantly less than the 1–2 MA loss for which there is some experimental evidence [1]. Nevertheless, this is substantially more than the 40 kA obtained in our previous calculations [2], where the radial MITL’s went out to only 14 cm. This

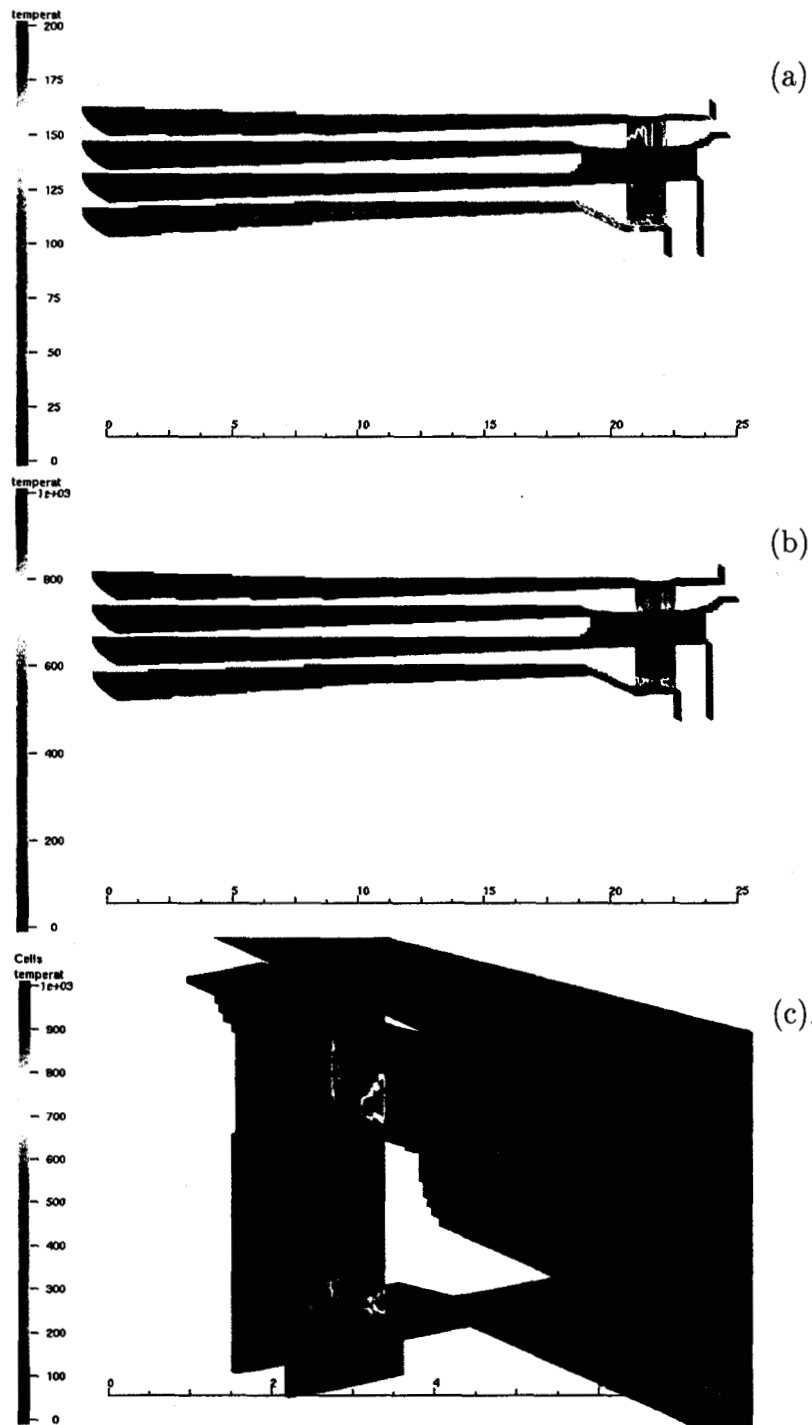
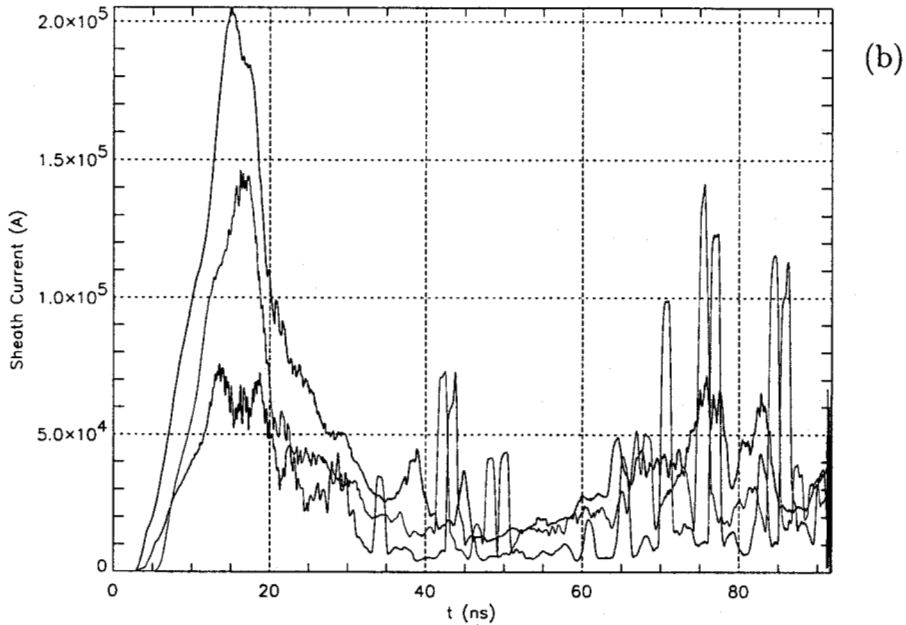
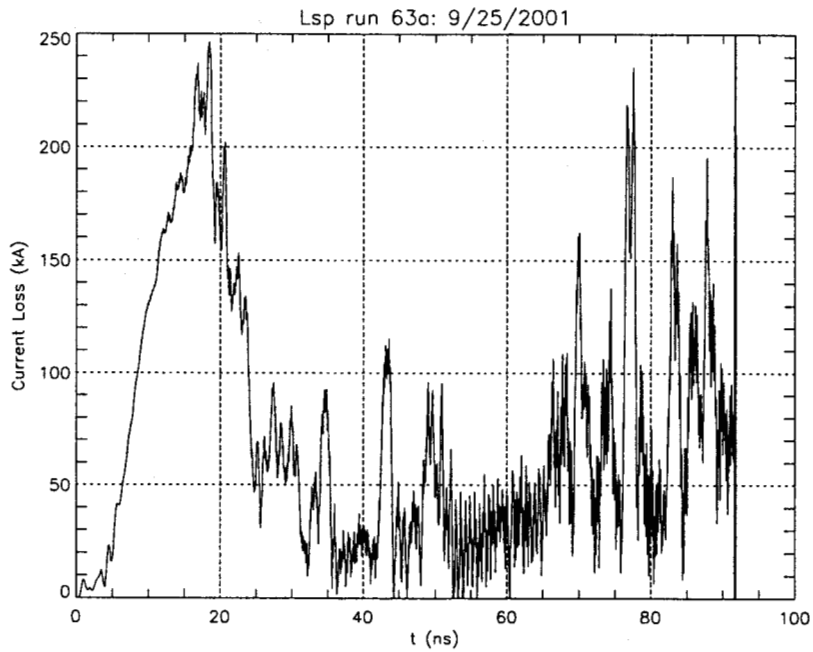


Figure 18: Color-coded plots of anode heating due to electron impact in 3-D calculation of convolute for two different temperature ranges: (a) 0–200 K and (b), (c) 0–1000 K. In (a) and (b) the outer radius (left) is at 30 cm, and the inner radius is at 4.4 cm from the central axis (larger than the actual inner radius on Z). Plot (c) is a close-up of the convolute from a different angle. The axes on the bottom are to show the scale (in cm) only.



PLOT LABELS  
 boxcar width=100  
 probe 55: flux J R at (2.00e+01 0.00e+00 9.80e+00) [half Z-convolute: input63a.lsp - Tue Sep 25 12  
 probe 56: flux J R at (1.50e+01 0.00e+00 9.80e+00) [half Z-convolute: input63a.lsp - Tue Sep 25 12  
 probe 14: flux J R at (1.00e+01 0.00e+00 9.60e+00) [half Z-convolute: input63a.lsp - Tue Sep 25 12

Figure 19: (a) Current loss and (b) electron sheath current as functions of time going through the convolute for simulation in Fig. 18.

indicates that extending the MITL's leads to more current being launched in the region out to about 20 cm, as we found in the 2-D simulations above.

The neutral desorption model in LSP is a commonly-used thermal model [11], where the number of adsorbed molecules per  $\text{cm}^2$  is given by

$$\frac{dN_a}{dt} = -\nu N_a e^{-Q_a/T} \quad (3)$$

where  $Q_a$  is the desorption activation energy in eV,  $T$  is the surface temperature in eV,  $N_a$  is the surface density of adsorbed molecules, and  $\nu$  is a rate constant (normally taken to be  $10^{13} \text{ s}^{-1}$ ). This formula assumes a desorption process which is first order in  $N_a$ . At room temperature, binding energies below about 0.9 eV can be considered "volatile" [11]. In the calculation, we have used a value of 0.6 eV, and taken the adsorbed layer to be 10 monolayers of  $\text{H}_2$  (where 1 monolayer  $\equiv 10^{15} \text{ cm}^{-2}$ ). Once the neutrals have desorbed, we allow them to become ionized by both sheath electrons and secondary electrons using gas-phase impact ionization cross-sections for  $\text{H}_2$  [12].

A series of snapshots of particle positions from the simulation is shown in Fig. 20. In Fig. 20(a), magnetic insulation has not yet been achieved. As mentioned above, this is partly a result of the shortened voltage pulse used to drive the MITL's; there is less current loss at early time with the longer waveform used in the 2-D calculations above, and in previous 3-D simulations [2]. In Fig 20(b), magnetic insulation is well-established in the outer radial MITL's. As in the 2-D calculations, some of the "excess" sheath current flowing into the higher impedance region near the convolute is returned to the cathode, and some is launched into the AK gap as predicted by the thin-layer model [5], but in the form of electron vortices rather than as a stable sheath. The trajectory of these vortices is roughly in accordance with the force-balance equation (Eq. 1), i.e., the impedance between their centroid location and the anode tends to remain constant; note the suppression of cathode-surface emission underneath the vortices.

The green points in Fig. 20 indicate thermally desorbed  $\text{H}_2$  neutrals. The regions of significant desorption correspond to the hottest regions in Fig. 18. Once the neutrals are liberated from the surface, subsequent electron vortices create  $\text{H}_2^+ - e^-$  pairs. For most of the calculation, the secondary electrons are immediately lost to the anode. Near peak current however, significant buildup of secondaries occurs on the downstream side of the post, as indicated in Fig. 20(d). Unfortunately, this local buildup in the number of secondary electrons caused LSP to exceed the available memory on the processor (the calculation was carried out on 53 processors on Janus), causing the run to terminate prematurely (at peak current instead of at peak implosion). LSP has a compile-time option to "combine" particles

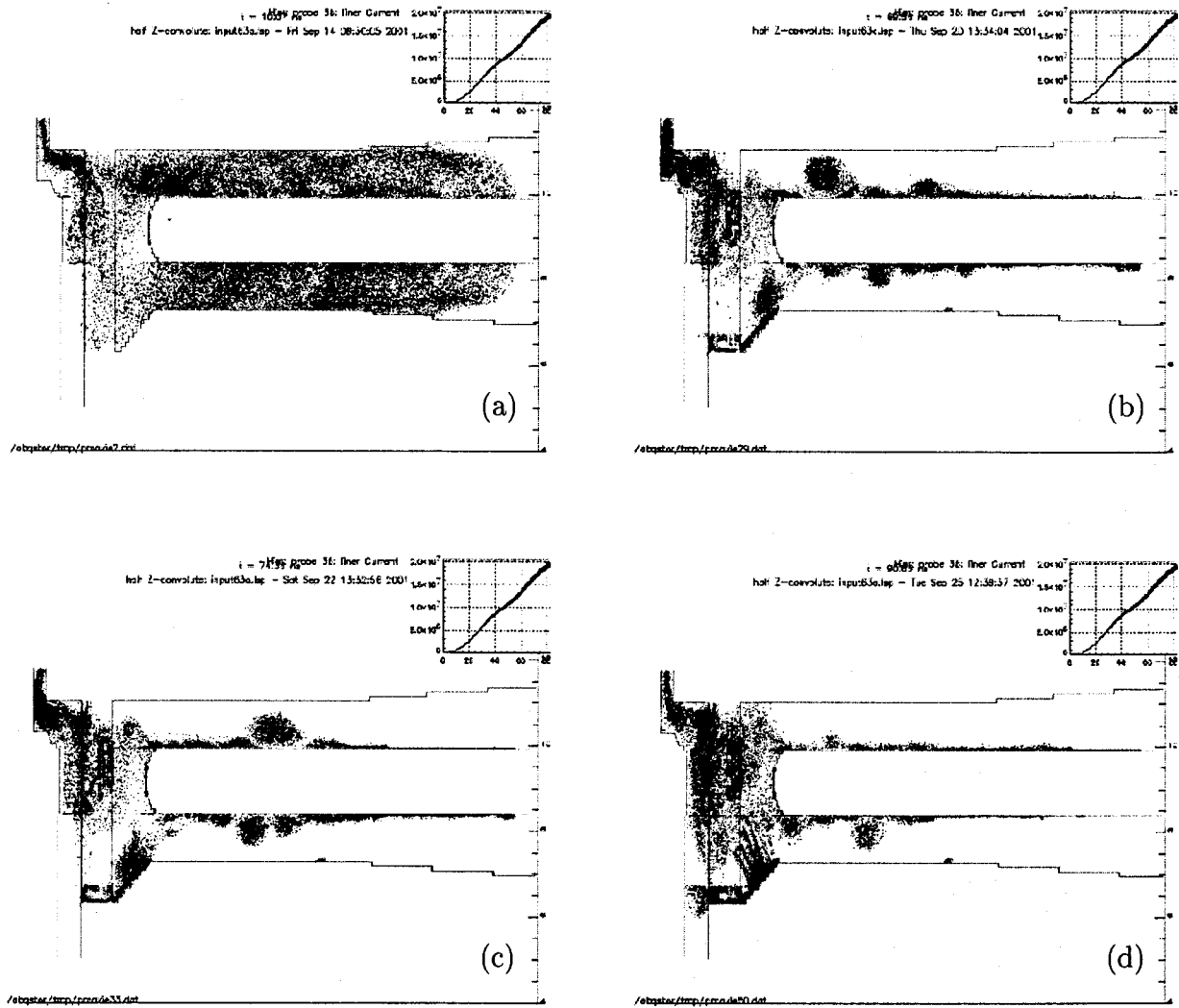


Figure 20: Snapshots of particle positions (projected onto the  $\theta = 0$  plane) from a 3-D simulation of convolute with neutral desorption /ionization.

to prevent local explosions in population, but we have not used this feature yet in convolute calculations.

The simulation indicates that avalanche breakdown of desorbed anode neutrals is possible in some places. Large 3-D simulations of this type are an inefficient way to study such processes, however. It may be possible to model the essential behavior in 1-D or 2-D geometries.

## 5 Cathode Plasmas

In the previous section, we saw that it may be possible to produce anode plasma in the convolute. We know for certain that cathode plasmas are formed on the MITL surfaces when the breakdown threshold is exceeded. Several millimeters of gap closure upstream of the convolute would significantly increase the sheath current (the local sheath current scales as  $1/a^2$ ). However, the plasma has to push against a strong transverse magnetic field, so that typical closure speeds of cm per microsecond may not be achieved. For the full-pulse simulation in Fig. 10, the magnetic pressure becomes larger than the plasma pressure ( $\beta < 1$ ) early in the pulse. The ratio of plasma pressure to magnetic-field pressure is given by:

$$\beta = \frac{8\pi nkT}{B^2} \simeq \frac{8 \times 10^5}{B^2 (\text{gauss})} \quad (n = 10^{16}/\text{cm}^3, T = 2 \text{ eV}) \quad (4)$$

where

$$B (\text{gauss}) = \frac{I(\text{A})}{5R (\text{cm})}$$

At  $R = 10$  cm, near the convolute,  $\beta < 1$  for  $I > 50$  kA, which occurs at  $t > 20$  ns while at  $R = 100$  cm,  $\beta < 1$  for  $I > 500$  kA, which occurs for  $t > 50$  ns. However, the plasma is resistive and the induced currents decay in a short time so values for  $\beta$  are misleading. Assuming Spitzer resistivity for a hydrogen plasma [13], we get a decay time

$$\tau_d = \frac{4\pi d^2}{c^2 \eta} \text{ s} \quad \text{where} \quad \eta = \frac{5.8 \times 10^{-14} \ln \Lambda}{T_e^{3/2} (\text{eV})} \text{ s}^{-1} \quad (5)$$

and  $d$  is the plasma thickness. For  $n_e = 10^{16} \text{ cm}^{-3}$ ,  $T_e = 2 \text{ eV}$  [11], we have  $\ln \Lambda \simeq 5.6$ ,  $\eta \simeq 1.1 \times 10^{-14} \text{ s}^{-1}$  and so  $\tau_d \simeq 0.12$  ns for  $d = 100 \mu\text{m}$ , much shorter than the 100 ns risetime of the current pulse.

To make an estimate of the forces on the plasma, consider a model where a uniform cold resistive plasma sheath is lying on a conducting surface (Fig. 21). If the magnetic field rises linearly in time,  $B_z(t) = \dot{B}_z t$ , and slowly enough that the field diffuses through the plasma on timescales of interest, the induced electric field and current are

$$E_x = \frac{1}{c} \dot{B}_z y \quad (6)$$

$$J_x = \sigma E_x = \frac{\sigma}{c} \dot{B}_z y \quad (7)$$

The force on the plasma per unit volume is

$$\frac{\mathbf{J} \times \mathbf{B}}{c} = -\frac{\sigma}{c^2} \dot{B}_z B_z y = -\frac{\sigma}{c^2} \dot{B}_z^2 t y \quad (8)$$

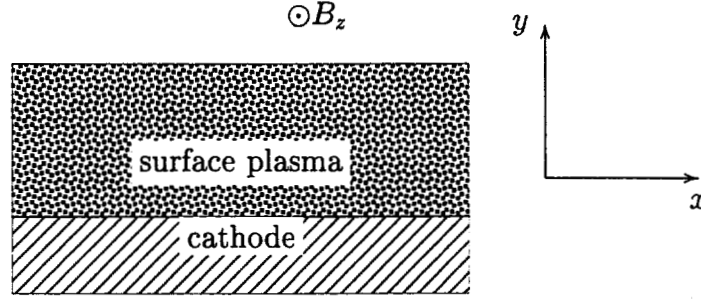


Figure 21: Schematic for calculation of forces on cathode plasma.

The magnetic diffusion causes ohmic heating of the plasma, generating a pressure (energy density) given by

$$P_{oh} = \mathbf{J} \cdot \mathbf{E}t = \frac{\sigma}{c^2} \dot{B}_z^2 y^2 t \quad (9)$$

Inside the plasma, the resulting force per unit volume is

$$-\frac{dP_{oh}}{dy} = -\frac{2\sigma}{c^2} \dot{B}_z^2 ty$$

which is in the same direction as the  $\mathbf{J} \times \mathbf{B}$  force. Comparing the pressure due to ohmic heating (Eq. 9) with the pressure due to the nominal initial plasma temperature, we find

$$nkT \simeq 3.2 \times 10^4 \text{ dyne/cm}^2 \quad (n_e = 10^{16} \text{ cm}^{-3}, T = 2 \text{ eV}) \quad (10)$$

$$P_{oh} \simeq 10^4 t \text{ (ns) dyne/cm}^2 \quad (11)$$

Thus, after just a few nanoseconds, the pressure is dominated by ohmic heating.

At the outer edge of the cathode plasma, the drop in density results in an outward force which is larger than the  $\mathbf{J} \times \mathbf{B}$  force by of order the ratio of the sheath thickness,  $d$ , to the length-scale of the pressure drop. Thus, for an initial sharp-edged plasma, the plasma boundary will accelerate outward at a rate unaffected by the magnetic field.

These considerations have motivated a closer look at cathode plasmas in the presence of a strong transverse magnetic field, which is presented in Appendix A.

## References

- [1] R. B. Spielman, W. A. Stygar, J. F. Seamen, F. Long, H. Ives, R. Garcia, and T. Wagoner, "Pulsed Power Performance of PBFA Z," p. 709; and K. W. Struve, T. H. Martin, R. B. Spielman, W. A. Stygar, P. A. Corcoran, and J. W. Douglas, "Circuit-code Modeling of the PBFA Z for Z-pinch Experiments," p. 162, Eleventh IEEE Pulsed Power Conference, IEEE Cat. No. 97CH36127, 1999.
- [2] T. P. Hughes and R. E. Clark, "3-D Calculations for the Z Double-Post-Hole Convolute, MRC/ABQ-R-1875, Mission Research Corporation, 1998; "3-D Simulation of Z Convolute for 120 ns Implosion Time," MRC/ABQ-R-2005, October 2000.
- [3] T. D. Pointon, W. A. Stygar, R. B. Spielman, H. C. Ives, and K. W. Struve, "Particle-in-cell simulations of electron flow in the post-hole convolute of the Z accelerator," *Phys. Plasma*, **8**, 4534, 2001.
- [4] J. Creedon, "Relativistic Brillouin Flow in the High  $\nu/\gamma$  Diode," *J. Appl. Phys.*, **46**, 2946-2955, 1975.
- [5] C. W. Mendel, Jr., D. B. Seidel, and S. E. Rosenthal, "A Simple Theory of Magnetic Insulation from Basic Physical Considerations," *Laser and Particle Beams*, **1**, 311, 1983.
- [6] M. S. Di Capua, "Magnetic Insulation," *IEEE Trans. Plasma Sci.*, **PS-11**, 205, 1983.
- [7] LSP is a product of Mission Research Corporation (<http://www.mrcabq.com/Services/Particle/Codes/codes.htm>).
- [8] C. W. Mendel, Jr., and S. E. Rosenthal, "Modeling Magnetically Insulated Devices Using Flow Impedance," *Phys. Plasmas*, **2**, 1332, 1995.
- [9] D. D. Hinshelwood, "Cathode Plasma Formation in Pulsed High Current Vacuum Diodes," *IEEE Trans. Plasma Sci.*, **PS-11**, 188, 1983.
- [10] R. W. Stinnett and T. Stanley, "Negative Ion Formation in Magnetically Insulated Transmission Lines," *J. Appl. Phys.*, **53**, 3819, 1982.
- [11] D. Lichtman in "Vacuum Physics and Technology," G. L. Weissler and R. W. Carlson, eds. (Academic Press, 1979), p.30.
- [12] C. F. Barnett, et al., "Atomic Data for Controlled Fusion Research," ORNL-5207, table C.4.2.
- [13] S. Glasstone and R. H. Lovberg, "Controlled Thermonuclear Reactions: An Introduction to Theory and Experiment," Van Nostrand, Princeton, 1960.
- [14] M. A. Mostrom, M. E. Jones and L. E. Thode, "Magnetically Insulated Plasma Sheath in Coaxial Transmission Lines with an External Magnetic Field," *J. Appl. Phys.*, **52** 1266, 1981.

- [15] C. W. Mendel, Jr., and S. E. Rosenthal, "Dynamic Modeling of Magnetically Insulated Transmission Line Systems," *Phys. Plasmas*, **3**, 4207, 1996.

# A MITL Cathode Plasma Modeling

Thomas C. Genoni, Thomas P. Hughes, and Bryan V. Oliver

## A.1 Introduction

We have begun an investigation of the behavior of resistive cathode plasma in a magnetically insulated transmission line. Such a plasma is a copious emitter of electrons and as it expands against the magnetic field it changes the effective anode-cathode gap, possibly resulting in gap closure. As a first step in this analysis we have developed a 1-D single fluid MHD model to describe the evolution of the cathode plasma in the presence of magnetic field diffusion and resistive plasma heating. A key feature of this model is the description of the plasma conductivity. We make use of an approximate analytic expression which includes contributions to plasma collisionality from coulomb interactions (Spitzer conductivity) as well as corrections due to turbulent motion which are of particular importance in the lower density regions of the plasma. The 1-D MHD equations and the plasma conductivity model are spelled out in Sections A.2 and A.3 below. In Section A.4 we present some initial numerical results for proton and  $C^{+3}$  plasmas expanding against magnetic fields ramping up to peak values of 5 and 10 tesla. Section A.5 contains a brief discussion of these preliminary results and some suggestions for possible future work.

## A.2 Single-Fluid 1-D MHD Equations

We consider a fully ionized plasma of ion density  $n$ , ion mass  $M = AM_p$  ( $A$  is the atomic weight and  $M_p$  the proton mass), charge state  $+Ze$  ( $e$  is the magnitude of the electronic charge), and electron density  $n_e = Zn$ . In our 1-D geometry we take the coordinate  $x$  to measure distance across the gap (from the cathode at  $x = 0$ ) and  $z$  to be in the direction of power flow so that the magnetic field  $B$  is in the  $y$  direction. We note that the ion velocity  $v = v_x$  and the plasma current  $j = j_z = (c/4\pi)\partial B_y/\partial x$  where  $c$  is the velocity of light. Under these conditions the single-fluid MHD equations take the form

$$M \frac{\partial n}{\partial t} = -\frac{\partial}{\partial x}(p) \quad (\text{A-1})$$

$$\frac{\partial p}{\partial t} = -\frac{\partial}{\partial x} \left( \frac{p^2}{Mn} + P + \frac{B^2}{8\pi} \right) \quad (\text{A-2})$$

$$\frac{\partial B}{\partial t} = -\frac{\partial}{\partial x}(vB) + \frac{c^2}{4\pi} \frac{\partial}{\partial x} \left( \frac{1}{\sigma} \frac{\partial B}{\partial x} \right) \quad (\text{A-3})$$

$$\frac{\partial P}{\partial t} = -\frac{\partial}{\partial x}(vP) - \frac{2}{3}P\frac{\partial v}{\partial x} + \frac{2}{3\sigma}j^2 \quad (\text{A-4})$$

where  $p = Mnv$  is the momentum density and  $P$  is the plasma pressure. We assume approximate equality of the electron and ion temperatures ( $T_e$  and  $T_i$  respectively) so that

$$P = n_e k_B T_e + n_i k_B T_i \simeq n(1 + Z)k_B T \quad (\text{A-5})$$

where  $k_B$  is Boltzmann's constant. The plasma conductivity  $\sigma$  is discussed in the next section.

### A.3 Plasma Conductivity Model

The plasma conductivity  $\sigma$  is given by

$$\sigma = \frac{n_e e^2}{m\nu_e} \quad (\text{A-6})$$

where  $m$  is the electron mass and  $\nu_e$  is the electron collision frequency. We take  $\nu_e$  to arise from coulomb interactions and from turbulent motion in the plasma; i.e.,

$$\nu_e = \nu_{ei} + \nu^* \quad (\text{A-7})$$

where

$$\nu_{ei} = \frac{2.9 \times 10^{-6} n \ln(\lambda)}{T(\text{eV})^{3/2}} \quad (\text{A-8})$$

is the familiar Spitzer (coulomb) collisionality and  $\nu^*$  is a low density turbulent correction. (In Eq. A-8 we ignore the weak density dependence of  $\lambda$  and set  $\ln(\lambda) = 10$ .)<sup>1</sup> Following Ichimaru<sup>2</sup> we take

$$\nu^* = \begin{cases} \nu_1^* = \frac{\sqrt{2}\Omega_e}{16\pi} \ln(M/m), & \alpha \gg 1 \\ \nu_2^* = \frac{\omega_{pe}}{4\pi\sqrt{2}\pi} \ln\left(\frac{M}{m}\right) \ln\frac{1}{\alpha}, & \alpha \ll 1 \end{cases} \quad (\text{A-9})$$

where

$$\alpha = \frac{2\omega_{pe}^2}{\Omega_e^2} \quad (\text{A-10})$$

and  $\omega_{pe}$  and  $\Omega_e$  are the electron plasma frequency and cyclotron frequency respectively:

$$\omega_{pe}^2 = \frac{4\pi n_e e^2}{m}, \quad (\text{A-11})$$

$$\Omega_e = \frac{eB}{mc}. \quad (\text{A-12})$$

The limiting forms for the collisionalities  $\nu_1^*$  and  $\nu_2^*$  correspond to anomalous electron collisions due to wave-particle interactions. In the case of  $\nu_1^*$ , the interaction is with cyclotron

waves and is therefore linearly dependent on the magnetic field strength  $B$ , whereas  $\nu_2^*$  is due to Langmuir wave oscillations and scales as  $\sqrt{n_e}$ .

In general, the anomalous collisionalities are only relevant when the relative drift velocities of the electrons and ions exceed the ion acoustic velocity, i.e.

$$v_i - v_e = \frac{j}{en_e} \gg \left(\frac{kT}{M}\right)^{1/2} \quad (\text{A-13})$$

For typical conditions in the low density plasma of the MITL,  $j = 10^6$  A/cm<sup>2</sup> and  $n_e \sim 10^{17}$  cm<sup>-3</sup> such that  $v_i - v_e \simeq 5 \times 10^7$  cm/s. For a 20 eV proton plasma  $\sqrt{kT/M} \simeq 5 \times 10^6$  cm/s, and the condition (A-13) is met. For the initial numerical calculations reported below the following simple analytic expression for  $\nu^*$  is used:

$$\nu^* \simeq \frac{\alpha}{1 + \alpha} \nu_1^* + \frac{1}{1 + \alpha} \nu_2^* . \quad (\text{A-14})$$

A plot of  $\nu^*$  and the conductivity  $\sigma$  in the  $(B, n)$  phase space for a 10 eV plasma are shown in Fig. A-1 a) and b), respectively. At low values of the magnetic field strength and high densities the conductivity is nearly Spitzer and of order  $\sim 3 \times 10^{14}$  s<sup>-1</sup>. It falls off to values of order 0.1 Spitzer ( $10^{13}$  s<sup>-1</sup>) in the low density, large field regime.

## A.4 Numerical Calculations

Equations A-1-A-4 are integrated forward in time on a fixed spatial grid in the coordinate  $x$  with 25  $\mu\text{m}$  resolution. Following Ref. 3 we use a variation of the two-step Lax-Wendroff method in which the magnetic diffusion term is ignored in calculating the auxiliary variables at the half time step, and brought in when the physical variables are calculated at the full time step. The scheme is explicit, thus small time steps are necessary to accommodate the relatively large values of  $1/\sigma$ . The initial conditions for each case below consisted of a stationary plasma sheath with a Gaussian profile of peak density  $n(x = 0) = 2 \times 10^{19}$  cm<sup>-3</sup> at the cathode, falling to 1/2 peak density at  $x = 100$   $\mu\text{m}$ . We choose the point at which the plasma density falls to  $10^{16}$  cm<sup>-3</sup> to represent the "edge" of the plasma beyond which vacuum conditions are obtained. Starting at  $t = 0$  the magnetic field ramps up from 0 to its maximum value (of 5 or 10 tesla) over the 100 ns period of the calculation.

Results for a proton plasma are shown in Figs. A-2-A-4. In Figs. A-2 and A-3, the evolution of the plasma density profile from  $t = 0$  to  $t = 100$  ns is shown. In both cases (peak  $B$  fields of 5 and 10 tesla) the magnetic field is effective in retarding the expansion of the bulk of the plasma, while at the same time, the low density plasma leading edge is able to

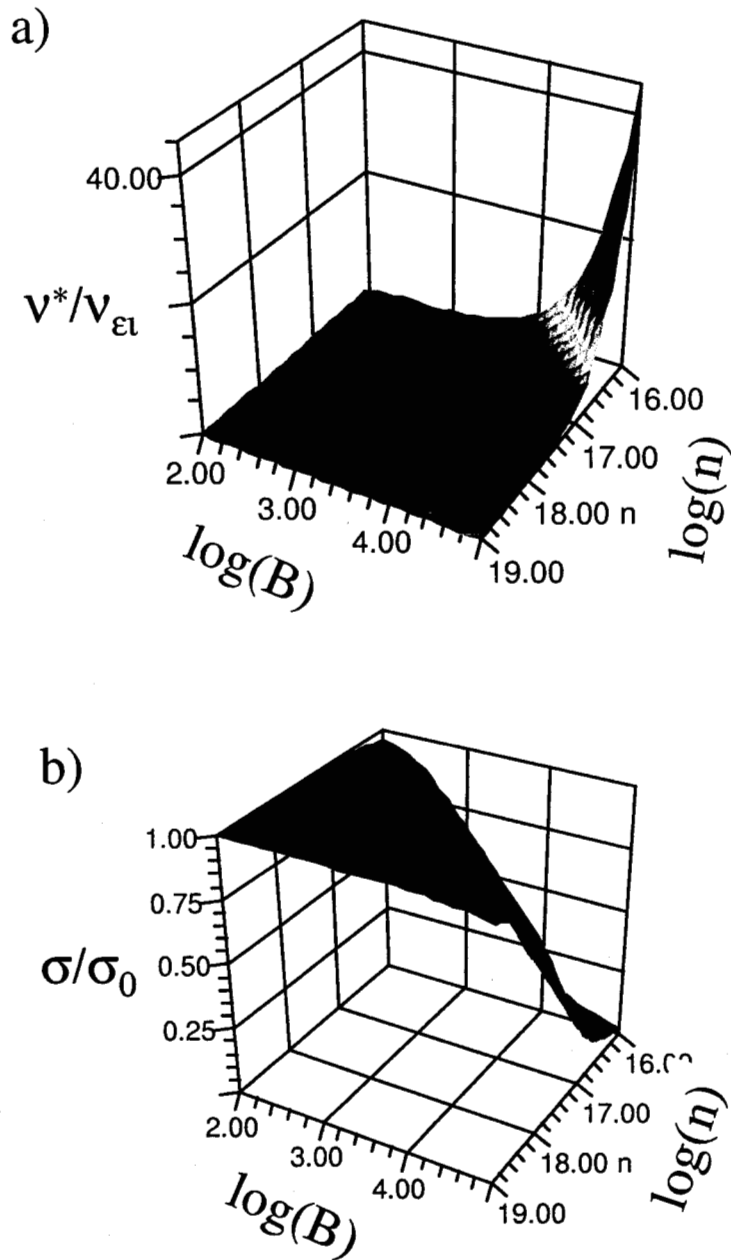


Figure A-1: The anomalous collisionality (a) and conductivity (b) as a function of the density  $n$  (in  $\text{cm}^{-3}$ ) and magnetic field  $B$  (in gauss). The collisionality is normalized by the Coulomb collision frequency  $\nu_{ei}$  and the conductivity by the Spitzer value  $\sigma_0 = (ne^2/mv_{ei})$ . A plasma temperature  $T = 10$  eV is assumed.

traverse a significant fraction of the 0.5 cm gap. Figure A-4 compares the  $t = 100$  ns plasma density profile against that which would have resulted from a free plasma expansion (against no  $B$  field). Results for a  $C^{+3}$  plasma are shown in Figs. A-5-A-6 for a peak magnetic field of 10 tesla. In this case, the magnetic field diffuses relatively freely through the higher  $Z$  (lower conductivity) plasma and has only a minor effect on the evolution of the plasma density profile.

## A.5 Summary and Discussion

The results presented here indicate the possibility of low density plasma expansion across the large magnetic fields found in the gap of the  $Z$  accelerator MITLs, upstream of the convolute. In the case of a proton plasma, with peak density  $n_i = 2 \times 10^{19} \text{ cm}^{-3}$  and initial width of  $\sim 100 \mu\text{m}$ , the plasma expands across 1/3 of the A-K gap or approximately 1.5 mm. Similar results are obtained for a carbon plasma in the +3 charge state. In both cases it is the leading edge of the plasma, with a density  $\sim 5 \times 10^{16} \text{ cm}^{-3}$  that travels the furthest distance, whereas the higher density region ( $\geq 10^{18} \text{ cm}^{-3}$ ) is eventually stopped and pushed back towards the cathode. In both cases, the expansion of the plasma is slower than the free expansion which would occur if no field were present. We note that compared to the high density, high atomic number plasmas expected to form from the heating of the metal cathode material (e.g., aluminum or copper), the plasmas considered here represent the "dirt" that most likely exists on the very surface of the metal. The numbers chosen for the initial conditions represent of order 2-5 monolayers of hydrogen or carbon.

Two important features allow for the expansion. First, the solid metal cathode that the plasma is in contact with provides an essential path for the current to flow, and the low density plasma need only carry a fraction of the total current (in the simulations, the solid metal cathode is modeled via the boundary condition). Thus, the current density and the corresponding  $\mathbf{j} \times \mathbf{B}$  force is small. Second, the diffusion time across a tenuous plasma of width  $a \simeq 250 \mu\text{m}$  is fast:  $\tau \simeq 2\pi\sigma a^2/c^2 \leq 0.5 \text{ ns}$  (for a good conducting plasma with  $\sigma = 10^{14} \text{ s}^{-1}$ ). This time is very short compared to typical current rise-times and one can expect the plasma to be unmagnetized for the bulk of the rise-time. Diffusion of the field through the plasma, heats the plasma, allowing for expansion due to thermal pressure. It moves across the field at a rate of expansion which is less, but still close to, its local sound speed. For a 10 eV hydrogen plasma, the sound speed is  $\sim 3 \times 10^6 \text{ cm/s}$ . Unimpeded the plasma would fully traverse 3 mm in 100 ns. The 1-D simulations suggest this speed is only reduced by a factor of two due to the magnetic field pressure. It is important to realize

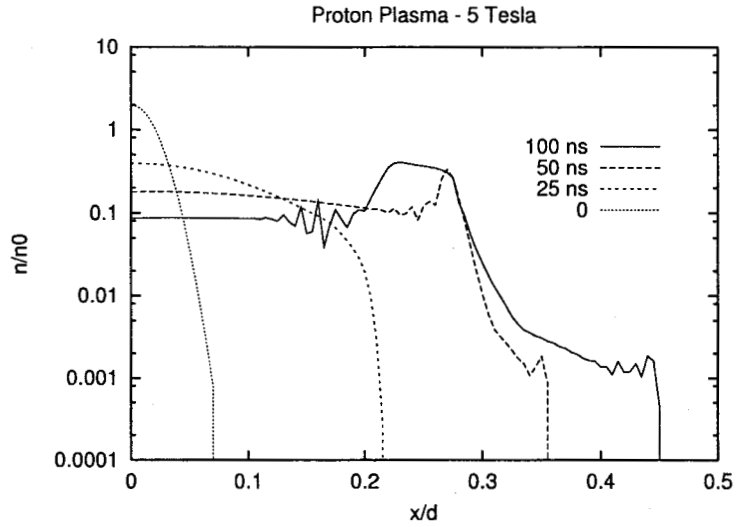


Figure A-2: Evolution of density profile of 1 eV proton plasma expanding against ramped magnetic field (peak 5 tesla).

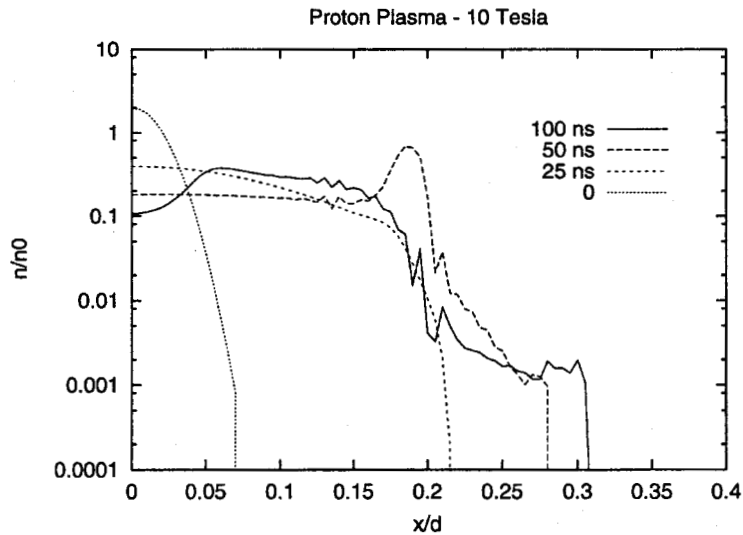


Figure A-3: Same as Fig. A-2 for peak magnetic field 10 tesla.

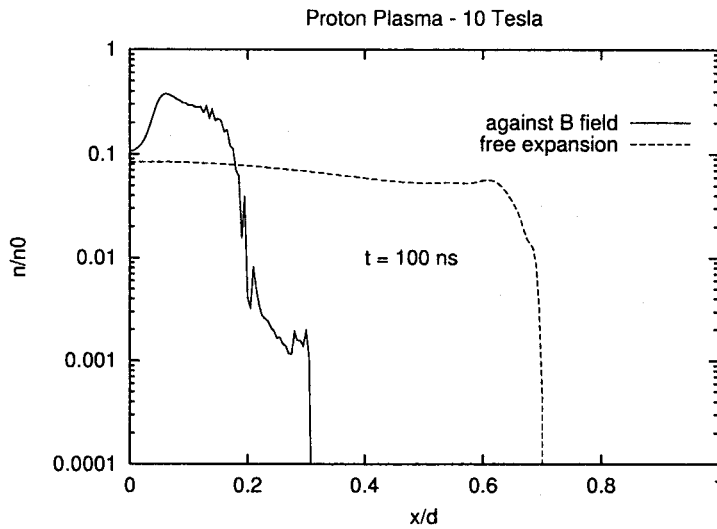


Figure A-4: Expansion of proton plasma at  $t = 100$  ns with and without ramped magnetic field (peak 10 tesla).

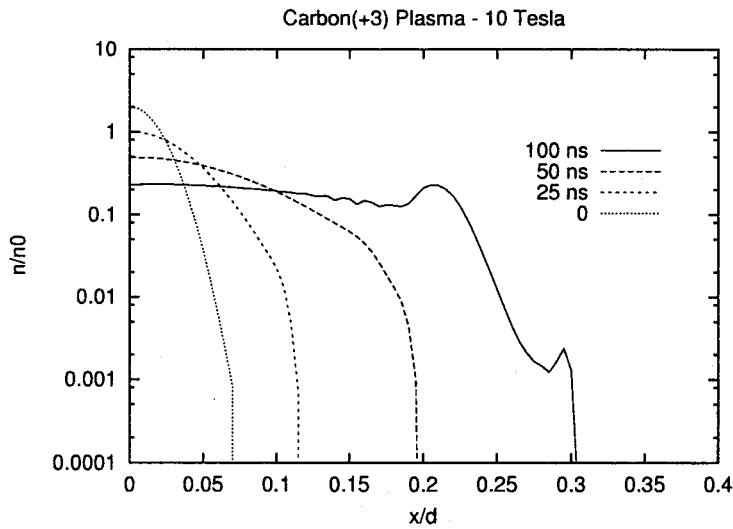


Figure A-5: Same as Fig. A-3 for 1 eV  $C^{+3}$  plasma.

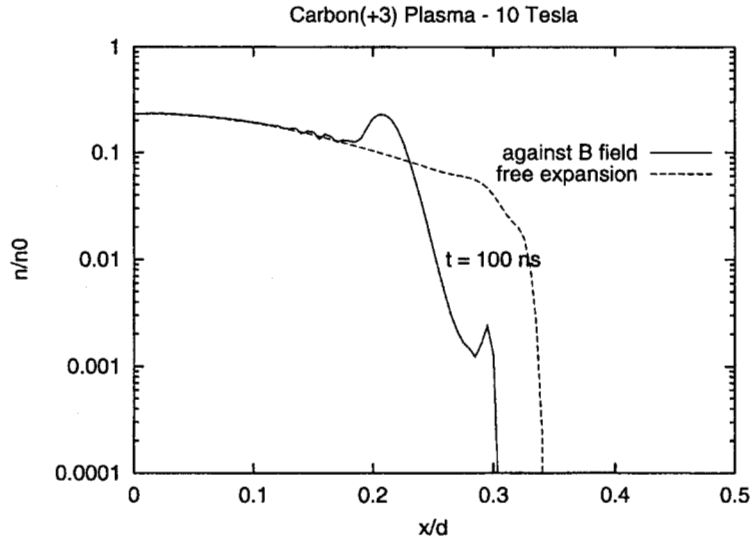


Figure A-6: Same as Fig. A-4 for 1 eV  $C^{+3}$  plasma.

that this fairly rapid expansion across the field occurs even though the plasma satisfies  $\beta = (8\pi nkT/B^2) \ll 1$  for the bulk of the rise-time.

Because the MITLs upstream of the convolute typically have gap widths of 5 mm, and the plasma expansion is of order 1.5 mm in 100 ns, the decreasing gap could be cause for decreased MITL impedance. It is unlikely, however, that such a mechanism would result in impedance collapse due to plasma closure. In addition, for higher current systems, the confinement of the plasma should be even better. Alternatively, similar physics should apply inside the gap just upstream of the  $Z$  pinch load. In this case, gaps of 1–2 mm are typically used and could exhibit collapse late in time. The weak scaling of the expansion rate vs. magnetic field seen in Figs. A-2 and A-3 (of order 30% reduction for a factor of 2 increase in field strength) suggests that even at the load, where field strengths are a factor of 8 times larger than at the convolute, closure of small gaps (e.g., 0.5 mm) is possible. This effect may be considered in greater detail in future studies.

## A.6 Acknowledgements

We thank W. Stygar and T. Pointon for valuable discussions concerning the  $Z$  accelerator and related MITL physics. Financial support has been provided by the U.S. Dept. of Energy, through Sandia National Laboratories.

## A.7 References

1. Francis F. Chen, *Introduction to Plasma Physics*, Plenum Press, New York, 1974, pp. 158-160.
2. S. Ichimaru, *Basic Principles of Plasma Physics, A Statistical Approach*, Addison-Wesley, Reading, MA, 1980, pp. 288-292.
3. K. V. Roberts and D. E. Potter, "Magnetohydrodynamic Calculations," in *Methods In Computational Physics Vol. 9*, Academic Press, New York, 1970, pp. 339-377.

# B Magnetically Insulated Electron Flow On $Z$ With Ions

Bryan V. Oliver, Robert E. Clark, and Thomas P. Hughes

## Abstract

The effect of background ion space-charge on the one dimensional, laminar, equilibria of relativistic, magnetically self-insulated electron flows is discussed. The theory is applied to describe the operating impedance of  $Z$  accelerator MITL's and estimate a possible mode of loss current for the accelerator. It is found that under standard operating conditions, the ion current density is order  $100 \text{ A/cm}^2$ , and the insulated electron current is increased by nearly a factor of two above the standard operating conditions without ions. At peak current operation the maximum electron current losses estimated from this process are of order  $\sim 100 \text{ kA}$ .

## B.1 Introduction

In the radial feed, magnetically insulated transmission lines (MITL) of the  $Z$  accelerator, loss currents of greater than 1 mega-ampere have been inferred from electrical characteristics. It is suspected that a primary contributor is the loss of the MITL insulated electron flow near magnetic nulls in the convolutes of the accelerator. However, the total current estimated in the electron flow under ideal conditions is typically of order 50 kA, well short of the measured 1 MA. Here we consider the possibility that the flow current could be enhanced by the presence of ions in the radial feeds. The presence of ions in the gap of the feeds not only act to carry excess current but to also alter the self-insulation characteristics of the MITL, increasing the amount of electron current in the flow, which can subsequently be lost in the convolute.

One dimensional (1-D), self-magnetically insulated electron flow is a well studied topic dating back to 1945 [1] and has been applied to studies of the operating impedances of high current diodes in the 1970's [2-4], and to magnetically insulated transmission lines in the 80's and 90's [5-7]. In these cases, 1-D equilibria are laminar  $\mathbf{E} \times \mathbf{B}$  drifts in the self-consistent electric and magnetic fields of the electron flow (including the contributions from the conducting boundaries). Here, we consider the previous theories in conjunction with MITL operation, but extend them to include the physics of a background ion space charge in the MITL anode-cathode (A-K) gap. An illustration of the geometry is given in Figure B-1.

In particular, we consider laminar flow equilibria for the electrons in the presence of ions when the background ion space-charge distribution is determined by space-charge limited emission from the anode. The ions are assumed unmagnetized (i.e., the ion trajectories are not altered by the magnetic field). The theory presented here has recently been used to describe the operating characteristics of self-insulated rod-pinch diodes [8].

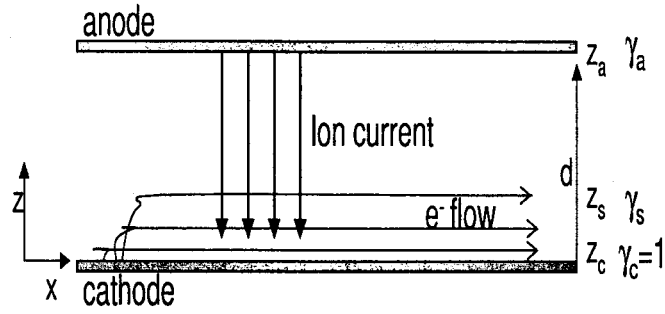


Figure B-1: Illustration of the cartesian equivalent radial feed MITL.

## B.2 Model Equations

The model geometry is illustrated in Figure 1. We assume the cartesian equivalent of the radial MITL's, with laminar ( $x$ -directed) electron flow in regions I, and axial ( $z$ -directed) ion flow in regions I and II. The self-insulating magnetic field is directed into the page ( $y$ -axis). The cathode, sheath and anode positions are denoted by  $z_c$ ,  $z_s$  and  $z_a$ , respectively (the A-K gap  $d = z_c - z_a$ ). We assume no variation in the  $x$  or  $y$ -direction of any of the quantities.

In the electron sheath region I ( $z_c \leq z \leq z_s$ ), the equilibrium equations are:

$$\begin{aligned}
 \frac{d^2\phi}{dz^2} &= n_e - n_i, \\
 \frac{dB}{dz} &= n_e v_e, \\
 \frac{d\phi}{dz} &= v_e B, \\
 \gamma - 1 &= \phi
 \end{aligned} \tag{B-1}$$

where  $\phi(z)$  is the electrostatic potential,  $n_e(z)$  and  $n_i(z)$  are the electron and ion number densities,  $v_e$  is the electron ( $x$ -directed) velocity,  $B$  is the azimuthal ( $y$ -directed) component of magnetic field, and  $\gamma = 1/\sqrt{1 - v_e^2}$  is the electron relativistic factor. Quantities have been normalized according to  $\phi = e\phi/mc^2$ ,  $B = eB/mc^2$ ,  $v = v/c$ ,  $n = 4\pi e^2 n/mc^2$ , where  $e$ ,  $m$  is the electron charge, mass and  $c$  is the speed of light (in the above normalizations, cgs units are used and the magnetic field has dimensions of inverse length). The equations (B-1) represent Poisson's, Ampere's, and the momentum equation, respectively in the steady state limit. The final equation is conservation of energy for the electrons, where we assume that on the cathode  $\phi_c = 0$  and all electrons are born with zero velocity ( $\gamma_c = 1$ ). We also explicitly assume only axial ion currents and thus, the ion current does not appear in Ampere's law. As will be shown below, the ion current is incorporated into the cathode boundary condition on the magnetic field  $B_c$ .

In region II ( $z_s \leq z \leq z_a$ ), only the ions are present and Poisson's and Ampere's equations become:

$$\frac{d^2\phi}{dz^2} = -n_i. \tag{B-2}$$

$$\frac{dB}{dx} = 0$$

The ion number density  $n_i$  is determined from continuity and conservation of energy

$$\begin{aligned} n_i v_i &= j \\ (M/Zm)v_i^2 &= 2(\phi_a - \phi) \end{aligned} \quad (\text{B-3})$$

where  $j$  is the normalized ( $4\pi e j / Z m c^3$ ) ion current density at the anode,  $v_i$  the ion velocity and  $M/Z$  the ion mass to charge ratio. The above equations may be combined to obtain a single differential equation for  $\gamma(z)$  in each region viz:

$$\begin{aligned} \gamma'' &= \frac{\gamma}{\gamma^2 - 1} (\gamma')^2 + (\gamma^2 - 1) \frac{K}{\sqrt{\gamma_a - \gamma}} \quad I \\ &= -\frac{K}{\sqrt{\gamma_a - \gamma}} \quad II \end{aligned} \quad (\text{B-4})$$

where  $K = (M/2Zm)^{1/2} j$  and ' denotes differentiation with respect to  $z$ . In the absence of ions  $K = 0$  and from Eq. (B-4) one retrieves the familiar differential equation describing magnetically insulated laminar electron flow in vacuum [3]. The boundary conditions on  $\gamma = 1 + e\phi/mc^2$  at the cathode and anode are  $\gamma_c = 1$  and  $\gamma_a = 1 + eV/mc^2$ , respectively (where  $V$  is the applied voltage). We also assume space-charge limited emission of the ions at the anode such that  $\gamma'_a = 0$ . The final boundary condition relates the magnetic field (or current) at the cathode to  $\gamma$  at the cathode viz:

$$B_c = \frac{\gamma_c \gamma'_c}{\sqrt{\gamma_c^2 - 1}}. \quad (\text{B-5})$$

Equation (B-4) has the first integral:

$$\gamma'_< = \sqrt{\gamma^2 - 1} \left[ B_c^2 + 4K \left( \sqrt{\gamma_a - 1} - \sqrt{\gamma_a - \gamma} \right) \right]^{1/2} \quad (\text{B-6})$$

$$\gamma'_> = 2\sqrt{K}(\gamma_a - \gamma)^{1/4}, \quad (\text{B-7})$$

where the boundary condition (B-5) has been utilized and the subscripts  $<, >$  refer to the regions  $I$  and  $II$ , respectively. Solutions to Eq. (B-6) and (B-7) in the limits relevant to  $Z$  accelerator parameters are discussed below.

### B.3 Limiting Solutions

Solutions to the equations are obtained via the matching conditions at the sheath location  $z_s$ , i.e.,  $\gamma_<(z_s) = \gamma_>(z_s)$  and  $\gamma'_<(z_s) = \gamma'_>(z_s)$ . Matching the derivative at  $z_s$  yields the following relationship for the cathode boundary field

$$B_c^2 = 4K \left( \frac{\gamma_s^2}{(\gamma_s^2 - 1)} (\gamma_a - \gamma_s)^{1/2} - (\gamma_a - 1)^{1/2} \right). \quad (\text{B-8})$$

For low impedance (relative to the MITL impedance), high current loads, such as occurs on  $Z$ , where the current running in the boundary greatly exceeds the flow current (i.e., the so-called "load limited" regime [6]), the sheath energy satisfies  $\gamma_s \simeq 1 \ll \gamma_a$ . In this regime, according to (B-8),  $B_c^2 \gg 4K$  or equivalently, the total boundary current is much larger than the ion current. In this limit, we can neglect the second term in the radical on the right-hand-side of Eq. (B-6) and integrate (B-6) and (B-7) to obtain

$$\gamma_{<} = \cosh(B_c(z - z_c)) \quad z \leq z_s \quad (\text{B-9})$$

$$\gamma_{>} = \gamma_a - K^{2/3} \left( \frac{3}{2}(z_a - z) \right)^{4/3} \quad z \geq z_s \quad (\text{B-10})$$

Matching  $\gamma$  at  $z = z_s$  and using the relation (B-8) to write  $K$  in terms of  $B_c$ , a final relation for the boundary current in terms of the sheath energy  $\gamma_s$  is retained:

$$B_c = \frac{1}{(z_a - z_c)} \left[ A \cosh(\gamma_s) - \frac{4(\gamma_a - \gamma_s)}{3\sqrt{\gamma_s^2 - 1}} F(\gamma_a, \gamma_s) \right] \quad (\text{B-11})$$

$$F(\gamma_a, \gamma_s) = \left[ \gamma_s^2 - (\gamma_s^2 - 1) \frac{\sqrt{\gamma_a - 1}}{\sqrt{\gamma_a - \gamma_s}} \right]^{1/2}.$$

The magnetic field at the anode  $B_a = (\gamma_s \gamma_s' / \sqrt{\gamma_s^2 - 1}) = \gamma_s B_c$ . The current (in Amps) in the radial feed MITL's is related to the field via  $I = I_A R B$ , where  $I_A = 8.5$  kA and  $R$  cm is the radial position in the feed. Hence the current in the anode  $I_a = \gamma_s I_c$  and satisfies

$$I_a = I_A g \gamma_s \left[ A \cosh(\gamma_s) - \frac{4(\gamma_a - \gamma_s)}{3\sqrt{\gamma_s^2 - 1}} F(\gamma_a, \gamma_s) \right], \quad (\text{B-12})$$

where  $g = R/d$  is the geometric factor and  $d = z_a - z_c$  is the MITL gap. In the appropriate limits of vanishing ion current  $K \rightarrow 0$ , the function  $F(\gamma_a, \gamma_s) \rightarrow 3/4$  and we retain the result of Creedon [3] for 1-D laminar, insulated flow current. The current flowing in the insulated electron flow (i.e., the sheath current) is just given by the difference between the anode and cathode currents  $I_s = I_a - I_c = I_a(\gamma_s - 1)/\gamma_s$ .

In Fig. B-2 the normalized anode current  $I/I_A g$  as a function of  $\gamma_s$  is plotted from Eq. (B-12) with  $\gamma_a = 5$  ( $V = 2$  MV). For comparison, also plotted is the similar graph for systems without ions. At 2 MV in the  $Z$  MITL's the total current is typically 5-5.5 MA per line and  $g = 10$ , suggesting a normalized current  $I/I_A g = 60-65$  and hence one will satisfy  $\gamma_s \simeq 1.0$ . In this limit,  $F(\gamma_a, \gamma_s) \rightarrow -1$  and for the same  $\gamma_s$ , the ratio of anode current with ions to the case without ions  $I_a/I_a^o \rightarrow 4/3$  (where the superscript  $o$  refers to the case without ion contribution). Alternatively, for similar total anode currents and voltages (i.e.,  $I_a = I_a^o$  in the same limit, the ratio of the sheath currents  $I_s/I_s^o = 16/9$ , implying that the presence of ions enhances the sheath current by nearly a factor of two and could contribute to excess current losses.

We note that the ion current density determined from Eq. (B-10) and the matching condition for  $\gamma$  results in a modified Child-Langmuir current  $j = (8/9)(\gamma_a - \gamma_s)^{3/2}/(x_a - x_s)^2$ .

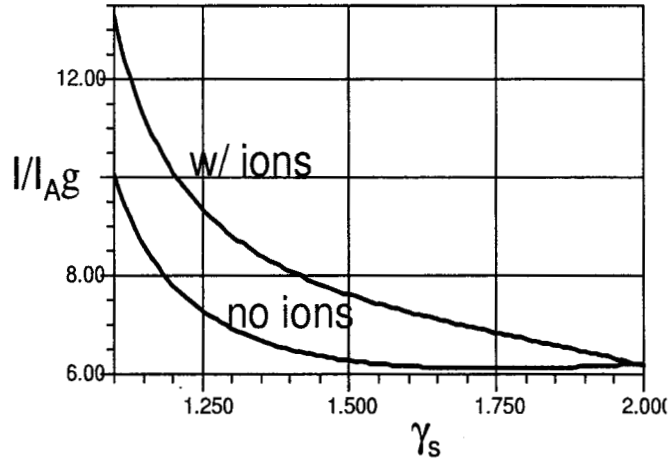


Figure B-2: Normalized MITL anode current as a function of  $\gamma_s$  with and without ions. The voltage  $V = 2$  MV.

In the limit  $\gamma_s \simeq 1$ , the ion current density (in cgs units) becomes the non-relativistic Child-Langmuir result

$$j \simeq j_{cl} = \frac{1}{9\pi} \sqrt{\frac{2Ze}{M}} \left( \frac{V^{3/2}}{d^2} \right). \quad (\text{B-13})$$

#### B.4 Estimated sheath currents for $Z$

There are two important operating phases in the radial feed MITL's of the  $Z$  accelerator. Early in time, e.g., 60 ns prior to peak current the MITL operates at currents which are approximately 5 times smaller than at peak current, we will call this the high impedance phase (termed 'hi'). Alternatively, at peak current the MITL is operating in a low impedance phase (termed 'lo'). In Fig. B-3, the normalized total current as a function of  $\gamma_s$  is plotted for a) high impedance and b) low impedance operations corresponding to voltages  $V = 1.3$  MV and  $V = 2.1$  MV, respectively.

When no ions are present [the limit  $F \rightarrow 3/4$  in Eq. (B-12)], in the high impedance phase, the anode current in a single feed is 1 MA at a radius  $R = 20$  cm and gap  $d = 1$  cm, giving  $g = 20$  and the normalized current  $(I/I_{Ag})_{hi} = 5.9$ , which yields  $\gamma_s^{hi} = 1.12$  (see Fig. B-3a). On the other hand, in the low impedance phase, the anode current is 2.1 MA, at a radius  $R = 10$  cm,  $d = 1$  cm, giving  $(I/I_{Ag})_{lo} = 63.5$  and  $\gamma_s^{lo} = 1.0022$  (see Fig. B-3b). The corresponding sheath currents in the two regimes are  $I_s^{hi} = 110$  kA and  $I_s^{lo} = 12$  kA, respectively. Since there are 4 MITL's which are joined at the convolute these flow currents, could represent current losses of upwards 440 kA at  $R = 20$  cm, and 48 kA ( $R = 10$  cm) respectively.

When ions are present the sheath currents are increased. According to Fig. B-3, for the same anode currents and operating voltages (i.e., same normalized current values) the

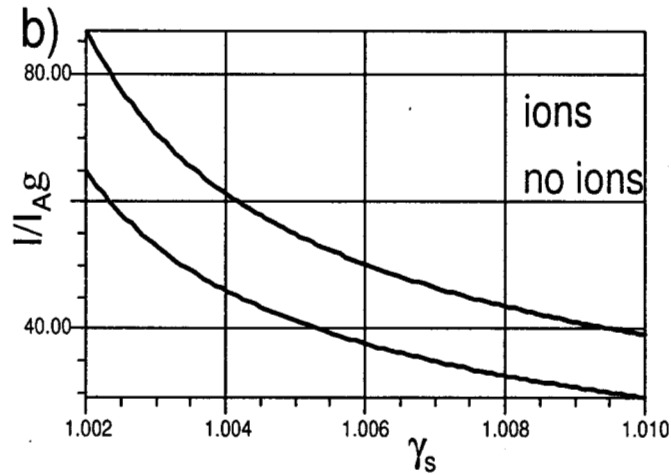
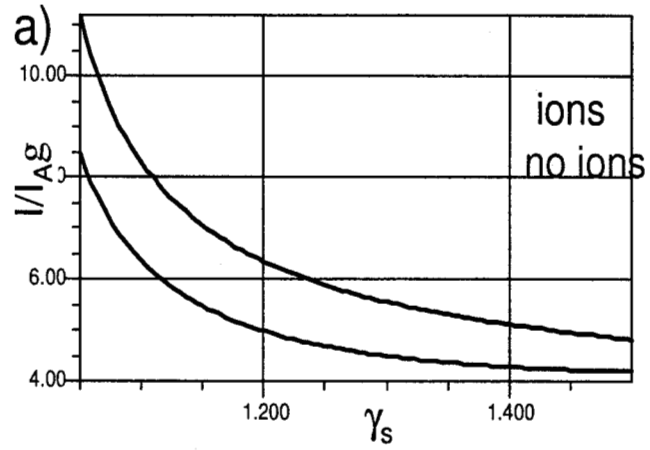


Figure B-3: Anode current vs.  $\gamma_s$  with and without ions for a) high impedance operation ( $I_a = 1$  MA,  $V = 1.3$  MV,  $g = 20$ ) and b) low impedance operation ( $I_a = 5.4$  MA,  $V = 2.1$  MV,  $g = 10$ ).

sheath energies are increased to  $\gamma_s^{hi} = 1.26$  and  $\gamma_s^{lo} = 1.004$ , which in turn yields  $I_s^{hi} = 206$  kA and  $I_s^{lo} = 21.5$  kA. Note that in both impedance cases, the system satisfies  $\gamma_s \sim 1$  and the scaling results presented above hold. In particular, the ratio of sheath currents with and without ions is  $\sim 16/9$ . Finally we note that in this same limit, the ion current density is given approximately by Eq. (B-13), yielding  $j^{hi} = 79$  A/cm<sup>2</sup> and  $j^{lo} = 164$  A/cm<sup>2</sup>, for the proton currents in the high and low impedance phases, respectively. These current densities are relatively small and would require in excess of 2000 cm<sup>2</sup> of ion emission area to account for approximately 1 MA of loss current due to ions.

## B.5 Conclusions

One dimensional, current equilibria in magnetically insulated transmission lines with the inclusion of ion current due to space-charge limited emission from the anode has been presented. The results suggests the possibility of decreased MITL impedances and a mechanism for increased electron losses. Typically, for the operating conditions of the Z accelerator, the cathode current is large and the equations for the equilibria can be simplified in the limit of strong insulation  $\gamma_s \sim 1$ . In this limit the current in the electron sheaths nearly doubles (16/9 times larger) over the sheath current values calculated without the presence of ions (i.e., the standard Creedon formulation). However, at peak current this still only amounts to approximately 20–25 kA of sheath current per MITL line and thus cannot account for the measured value of nearly 1 MA of loss current. Alternatively, at early times in the pulse (the so-called high impedance phase), total electron sheath currents could approach 800 kA at large radius  $R = 20$  cm. If this flow is not retrapped at small radius it could account for substantial loss current (at least for some time prior to peak current). If ions are present in the line, the ion current density will be nearly determined by Child-Langmuir flow. This corresponds to  $j \simeq 100$  A/cm<sup>2</sup> for typical MITL voltages on Z. Unless anomalously large areas of the MITLs emit ions, (e.g.,  $2 \times 10^3$  cm<sup>2</sup>) it is not expected that ion currents are the cause for loss currents in excess of 1 MA.

## B.6 Acknowledgements

We thank W. Stygar and T. Pointon at Sandia National Laboratories (SNL) for encouraging study of this problem. Financial support has been provided by the U.S. Department of Energy through Sandia National Laboratories.

## References

- [1] L. Brillouin, Phys. Rev. **67**, 620 (1945)
- [2] A. Ron, A. A. Mondelli, and R. N. Rostoker, Phy. Sci. **1**, 85 (1973).
- [3] John M. Creedon, J. Appl. Phys. **46**, 2946 (1975).

- [4] M. Reiser, Phys. Fluids **20**, 477 (1977).
- [5] C. W. Mendel, Jr., D. B. Seidel, and S. A. Slutz, Phys. Fluids **26**, 3628 (1983).
- [6] C. W. Mendel, Jr. and S. E. Rosenthal, Phys. Plasmas **2**, 1332 (1995).
- [7] B. W. Church and R. N. Sudan, Phys. Plasmas **2**, 1837 (1995).
- [8] B. V. Oliver, T. C. Genoni, D. V. Rose, and D. R. Welch, "The Impedance Characteristics of a Rod-Pinch Diode," Proc. of the IEEE Pulsed Power and Plasma Science Conference, June (2001).

# C Negative-Ion Current on the Z Machine

## Richard St. John

### Introduction and Summary

This quick look estimates the loss in the Z machine from the formation of negative ions in the cathode plasma. The total current loss to be explained is approximately 1 MA over an approximate cathode area of 20 m<sup>2</sup> (two, triplate transmission surfaces yield 4 times the physical area of a 1.3-m disk). This gives a surface current of about 5 A/cm<sup>2</sup> to be found. Information from two references is used<sup>1,2</sup>. A possible constraint in the loss is a measurement between the 20 and 80 cm locations of the Z machine indicating the losses are predominantly within the 20 cm radius. This requires substantially higher ion-current densities with a radial dependence to explain the observed losses (i.e., the losses are mostly within the 20 cm radius).

They conclude (in reference 1) that the ion current is associated with hydrogen, carbon, and oxygen and is limited to surface irregularities. The current density is a sensitive function of voltage rise rates and precursor voltages. Even if the current densities for different ion species are ill defined, the reference definitely shows that the current exists. There is a comment on the probability of a sufficient ion current to form an anode plasma with a possible catastrophic failure in the insulation. There are no hard results in this reference to apply to the Z machine current losses other than the fact that the negative-ion currents exist.

There are two types of negative-ion-current generation in reference 2. The first looks at predictions of negative ion production using neutral-particle production rates, electron and neutral-particle densities, electron velocities, and negative-ion production rates. These can vary over values that will easily supply the required 5 A/cm<sup>2</sup> and, just as easily, predict negative-ion currents that are negligibly small. Because no current losses in the Z machine are observed between 20 and 80 cm from the load, if there is a loss due to negative ions, it must be close to the load. Variations in the parameters can still explain the loss over a smaller area.

Hardware required to take the measurements of the negative-ion currents in the references tends to affect the actual density such that average densities are much smaller than measured values. It is possible that the observed currents are atypical and not representative of the normal behavior along the transmission line.

The second current-generation technique in reference 2 derives a dependence of the hydrogen ion current on the cube of the current density. Although the resulting negative-ion current was negligible in the accelerators in the reference's test, a comparison with

---

<sup>1</sup> J.P. VanDevender, R.W. Stinnett, and R.J. Anderson, "Negative ion losses in magnetically insulated vacuum gaps", *Appl. Phys Let.* **38**(4), 15 February 1981, p. 229

<sup>2</sup> Regan W. Stinnett and Tim Stanley, "Negative ion formation in magnetically insulated transmission lines", *J. Appl. Phys.* **53**(5), May 1982, p. 3819.

the current densities seen in the Z machine can lead to increases in the hydrogen by over two orders of magnitude. If this scaling relationship holds, it could explain both the current loss in the Z machine as a negative-ion flow and explain why the loss is inside the 20 cm radius.

### Discussion

Two papers (references 1 and 2) in the early 1980's discuss the formation of a negative-ion current in a magnetically insulated transmission line. Both deal with the two modular prototypes, Mite and Hydramite, of the Particle Beam Fusion Accelerator (PBFA) I. They portray a convincing presence of negative-ion currents for H, C, O, and heavier elements. The technique to show the presence of negative ions is current detected by a Faraday cup in the anode with and without shielding to stop the ions (but not any electron flow). The identification of the ion species is made with time-of-flight measurements with a sample shown in Figure C-1; the techniques employed in reference 2 use both a spectrometer and a Thompson Parabola Charged Particle Analyzer and report essentially the same ions. Carbon is present in these from a 25  $\mu$  graphite coating on both the cathode and anode in these modules: this is not present in the Z machine to as great an extent and ions are limited to mostly those in leftover water, presumably the source of the hydrogen and oxygen seen in the ion spectroscopy.

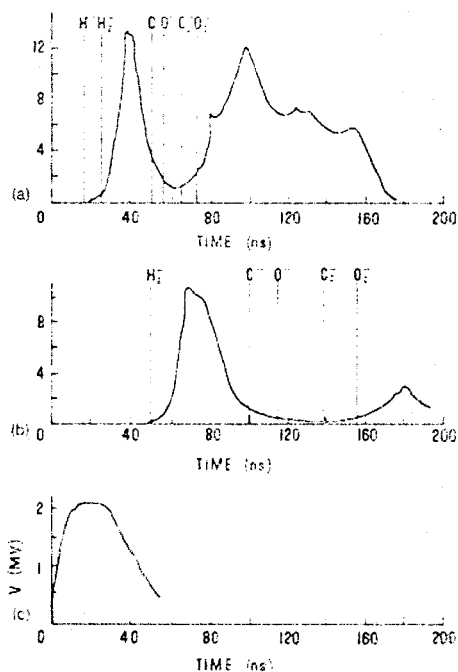


**Figure C-1. Time-of-flight measurements in reference 1 for 25 cm (a) and 55 cm (b) drift-tube lengths. The computed earliest arrival times for 2 MeV energies are noted for several ions (vertical axis is arbitrary units). The voltage is shown in (c) (reference 1).**

Reference 1 is the earlier of the two articles and attributes different ion current densities to different rise rates of the voltage pulse. In this reference, with a rise rate of  $1.4 \times 10^{14}$

V/s, the current density is as much as 20 A/cm<sup>2</sup>. With higher rise rates, the current falls to 2 A/cm<sup>2</sup>. Comparison with the voltage rise rates in the Z machine, a peak of about 10<sup>14</sup> V/s, the ion currents would tend to be larger than with a faster rise rate.

The transmission lines in the references are fixed at a 1-cm spacing. If the ion-current density is dependent on the rise rate of the electric field (which seems more likely), the production rate will be a function of position in the Z machine. The fields in the reference modules are over a centimeter implying a rise rate of 1.4x10<sup>16</sup> V/m/s yields 20 A/cm<sup>2</sup>. The Z machine has a rise rate of 10<sup>16</sup> V/m/s at a 1-cm separation falling to 2x10<sup>15</sup> V/m/s at a 5-cm separation. The Z machine rise rates are both smaller than the referenced rise rate and therefore would yield at least 20 A/cm<sup>2</sup>. This is well above the necessary amount to explain the 1 MA loss.

This argument appears weak and is certainly not quantifiable with any reasonable accuracy.

The peak current density in both modules is estimated from a 400 kA peak flowing on a triplate line with an effective width of 50 cm<sup>3</sup>. This reduces to a current density of 800 kA/m.

A second set of ion-current measurements gave a sufficiently large answer that the authors conclude the current is local to the Faraday cup (and possibly other sparse locations). This was based on the observation that the input and output currents of the module did not show sufficient disagreement to account for the measured ion flux over the entire surface area of the transmission line.

They conclude (in reference 1) that the ion current is associated with surface irregularities and the current density is a sensitive function of voltage rise rates and precursor voltages. Even if the current densities for different ion species is ill defined, the reference definitely shows that the current exists. There is a comment on the probability of a sufficient ion current to form an anode plasma with a possible catastrophic failure in the insulation.

The second reference quotes the following numbers for fields above 25 MV/m:

**Table C- 1. Approximate cathode plasma parameters for fields above 25 MV/m (reference 2).**

Electron density near cathode	10 <sup>24</sup> /m <sup>3</sup>
Electron density near outer edge of plasma sheath	10 <sup>20</sup> /m <sup>3</sup>
Source density of neutral atoms	10 <sup>20</sup> /m <sup>2</sup>
Plasma temperature	Several eV

<sup>3</sup> It's not obvious what is meant by "effective" in this reference. It will be interpreted here that the physical plate is about 20 cm wide and 5 cm thick. The current flows on both sides and edges giving an "effective" width of 50 cm.

These numbers can lead to the formation of negative ions with a detachment rate that is much higher than the attachment rate (reference 2). The field of 200 MV/m, however, can accelerate  $H^-$  across a 1-cm gap in about a nanosecond with a correspondingly longer time for the heavier ions. Since this is small compared to the collision time, a high percentage of all negative ions that are created will reach the anode (reference 2).

### Current Generation Technique #1

A cross section, suggested in reference 2, that could be responsible for significant ion production is the  $4 \times 10^{-16} \text{ cm}^2$  value for excited  $H_2$  interacting with an electron. With an appropriate density of molecular hydrogen or the presence of other neutral molecules with similar cross sections for the production of  $X_2^-$ , a large current could be explained.

Looking at this cross section and the values in Table C- 1, we can find a collision frequency for the formation of ionized  $H_2$  and a current loss for the Z machine. The rate of formation of negative ions is

$$r_{ion} \text{ (number/volume/second)} = N_n X_{M_2+e^- \rightarrow M_2^-} N_e v_e$$

where

$N_n$  is the density of neutral atoms and molecules

$X_{M_2+e^- \rightarrow M_2^-}$  is the cross section for electron collisions with molecules

$N_e$  is the electron density

$v_e$  is the electron velocity

If this rate occurs over the thickness of the plasma,  $t_p$ , the current density of ions is

$$I(A/area) = N_n X_{M_2+e^- \rightarrow M_2^-} N_e v_e t_p q_e$$

Looking carefully at each number, we have

$N_n$  is related to the  $10^{20}$  formed per square meter. The velocity of a 2 eV proton is about 20 km/s. During 100 ns, the proton could travel at most about 2 mm; this gives a minimum density of the neutral atoms of

$$N_n \geq 5 \cdot 10^{22} /m^3$$

The cross section is given in reference 2 and will be accepted at face value for this calculation. This is a value applicable only to excited  $H_2$  and is at least 4 orders of magnitude larger than that of the unexcited molecule.

$$X_{M_2+e^- \rightarrow M_2^-} = 4 \cdot 10^{-20} \text{ m}^2$$

The electron density is given in reference 2. Close to the cathode it is about  $10^{24} / \text{m}^3$  and at the edge of the plasma it is about  $10^{20} / \text{m}^3$ .

$$N_e \geq 10^{20} / \text{m}^3$$

The electron velocity is defined from the plasma temperature of 2 eV given in reference 2. This is about a factor of 30 smaller than one gets by looking at the cycloidal motion of free electron in the fields of the Z machine

$$v_e \geq 8 \cdot 10^5 \text{ m/s}$$

The final parameter is the thickness of the plasma where the collisional attachment occurs. It is assumed to be 100  $\mu$ ; this is about twice the cycloidal diameter expected in the Z machine.

$$t_p \approx 10^{-4} \text{ m}$$

Using the accepted value for the magnitude of the charge on an electron,  $1.6 \times 10^{-19} \text{ C}$ , the total current is about

$$I_{ion} \geq 2.5 \text{ MA/m}^2 \text{ or over } 50 \text{ MA ion-current loss.}$$

This is comparable to the total current and would be easily discernable. The corresponding  $250 \text{ A/cm}^2$  is about two orders of magnitude larger than the current necessary to explain the loss of 1 MA. With one simple change in the estimate: the actual cross section of the hydrogen molecule (or other neutral atom or molecule) is really 4 orders of magnitude less. This gives  $25 \text{ mA/cm}^2$ , an amount too small to account for the 1 MA discrepancy.

Using these numbers gives plenty of leeway to explain just about any current loss one would want to. However, measurements of current loss between the 80 cm and 20 cm points showed the Z machine's 1 MA was not lost in that area. This would require the ion loss to be inside the 20 cm mark; the numbers in reference 2 could still easily cover the current loss over the smaller area. Now, one would only have to explain why ions were active near the center and not near the edges when both areas see fields in excess of 25 MV/m.

### Current Generation Technique #2

A second explanation in reference 2 is the production of negative ions through backscattering plasma ions from the cathode surface. This source is most practical at a few eV (the temperature of the Z-machine plasma) and can yield about  $1 \text{ A/cm}^2$ : a value not too far from the required  $5 \text{ A/cm}^2$ . Measurements of ion-current densities in this reference are given in Figure C-2. This shows the combined ion current for H<sup>-</sup>, C<sup>-</sup>, and

$C_2^-$  are near the total of  $5 \text{ A/cm}^2$  required to explain the 1 MA loss in the Z machine (as discussed below, these current densities may not be representative of the average over the cathode).

The carbon-ion production in reference 2 shows a dependence on shot number after first applying a fresh carbon layer. Examination of the line after more than 25 pulses revealed that the cathode carbon directly opposite the ion spectrometer on the anode was depleted; carbon elsewhere on the line was still abundant. This points out that the negative-ion density can be extremely variable over the area of the cathode and the measured values seem to be a peak because of the field perturbation afforded by the detector. There is no mention of the repeatability of the ionized hydrogen current.

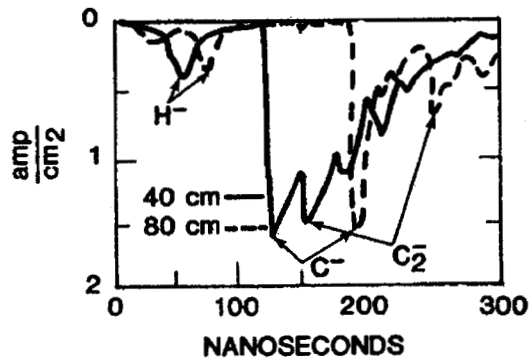


Figure C-2. Time-of-flight measurements and current densities for 40 cm and 80 cm drift tubes (reference 2).

The results of this give an upper limit to the ion current. In Figure C-3, the decrease in the carbon current is shown as the number of shots increases. There is a possibility that the  $H^-$  current is stable and represents the bulk of the remainder.

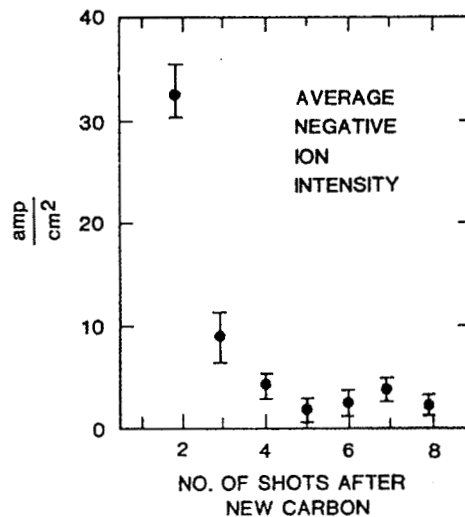


Figure C-3. Negative-ion current decrease with shot number (reference 2).

Extrapolation of the observed current density over the entire area of the cathode of the MITE module yields 77 kA, a loss that should easily be observed. This lends credence to the proposed sparseness of negative-ion production and its enhancement near the detector (reference 2). The conclusion in this reference is there is not sufficient ion production to affect the current propagation on the line. Unfortunately, these results give only an upper limit to the average negative-ion current that is about a factor of three less than that observed: this appears to be about  $1 \text{ A/cm}^2$ .

Further analysis is undertaken in reference 2: this examines the hydrogen ion current as a function of the total current. Theoretical research indicates the negative-ion production scales with the plasma temperature; the relationship with current was investigated to determine the major parameter responsible for the creation of negative ions. Their analysis shows an  $\text{H}^-$  current density scaling as the cube of the total current (Figure C-4). Similar behavior was seen in their ion densities during shots that were shorted. In the reference they conclude there is not a strong dependence of negative-ion production on voltage; it is due at least partially to the cathode plasma temperature as a function of the total current density.

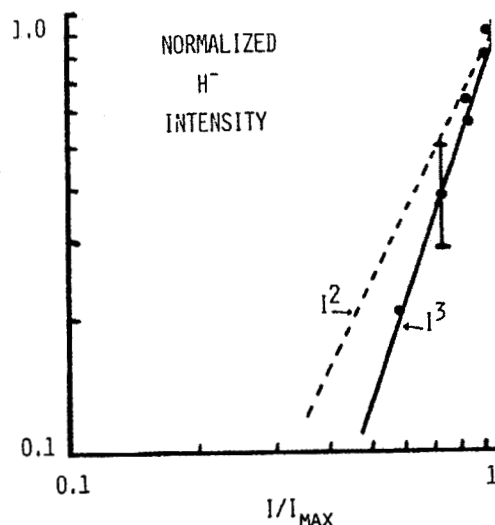
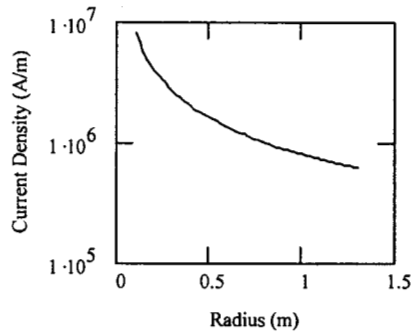


Figure C-4. Dependence of negative H ions on total current (reference 2).

The current density on the accelerator modules in references 1 and 2 is about 800 kA/m. The current density in the Z machine is a function of radius and is shown approximately in Figure C-5. At the outside of the vacuum section, the current densities are comparable with those in the references; at 20 cm from the center, the current density is 4 MA/m, about 5 times as large as that in the MITE and hydramite modules. If the  $\text{H}^-$  current density scales as the cube of this density, it is more than two orders of magnitude greater than it was on the outside radius of the cathode. If this scaling relationship holds, it could explain both the current loss in the Z machine as a negative-ion flow and explain why the loss is inside the 20 cm radius. Again, because the measured results in the references



**Figure C-5. Current density on each side of the Z machine cathode plates.**

were upper limits, only an upper limit can be assumed for the Z machine: this would be no more than  $100 \text{ A/cm}^2$  inside the 20 cm radius. At  $100 \text{ A/cm}^2$ , the loss radius would have to be over 50 cm to give a 1 MA current, a physical impossibility. However, since the  $H^-$  current density may scale as the cube of the current density, it may increase enough to deliver the 1 MA.

## **D Approximate Effect of Synchrotron Losses on a Magnetically Insulated Transmission Line**

**Richard St. John**

A Magnetically Insulated Transmission Line (MITL) employs the magnetic field parallel to the surface of a current-carrying conductor to impede the flow of electrons from the negatively charged surface to the positive one. Typically, the electrons orbit above the cathode in cycloidal orbits and drift in a direction perpendicular to both the magnetic and electric fields produced between the conductors; the direction of drift adds to the current on the transmission line. Because the electrons are accelerated, they will radiate and lose energy: this results in another, smaller drift velocity toward the positive plate and introduces the potential for a loss of the magnetically induced insulation.

The following is a nonrelativistic evaluation of this radiation-loss drift. For transmission-line values of 100 MV/m and 5 T, the results show the radiation-loss drift velocity of the electrons from the cathode to the anode is a leisurely 0.1 mm/s; this will not effectively circumvent the magnetic insulation for short pulses.

The analysis begins with the forces acting on a moving charge. This gives an acceleration on a free electron between the conducting surfaces of the transmission line as

$$\vec{a} = \frac{q_e}{m_e} (\vec{E} + \vec{v} \times \vec{B})$$

where all values are in mks units. For the geometry below in the absence of radiation losses, the orbit of a single electron in a 100 MV/m electric and 5 T magnetic field is given in Figure D-1. In this example, the electron starts at rest on the bottom conductor and drifts to the left from its starting position at  $x = 0$ .

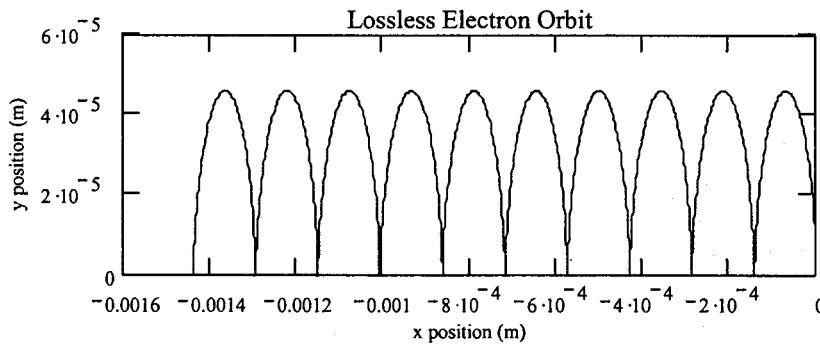
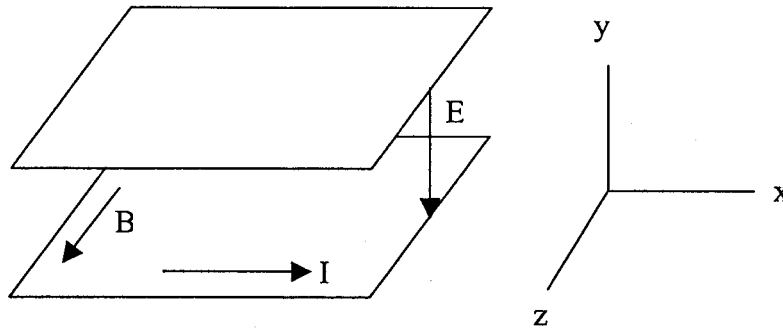


**Figure D-1. Orbit of single electron without radiation losses (motion is right to left for  $E_y = -100$  MV/m and  $B_z = 5$  T)**

The orbital parameters are found from the peak velocity of the electron at the top of its cycloid,

$$2E = v_e B \Rightarrow v_e = \frac{2E}{B} \quad (\text{about } 4 \times 10^7 \text{ m/s for } E=100 \text{ MV/m and } B=5 \text{ T})$$

The factor of 2 comes from the symmetry requirement that the magnetic force be twice that of the electric force to accelerate the charge back to  $y = 0$  (or, alternatively, the cycloidal velocity at the top is twice the average velocity). The derived velocity for the electric and magnetic field used in the example indicates the electron is sufficiently far from the relativistic regime to allow the use of classical approaches ( $\gamma = 1.009$ ). Note, however, that a factor of several increase in the electric field and a factor of several decrease in the magnetic field could easily push the electron into relativistic velocities.

Equating the potential and kinetic energies of the electron at the top of the cycloid gives the maximum excursion in the y direction,

$$\frac{1}{2} m_e v^2 = q_e E y_{\max} \Rightarrow y_{\max} = \frac{2m_e E}{q_e B^2} \quad (\text{about } 45 \mu \text{ for } E=100 \text{ MV/m and } B=5 \text{ T})$$

with a period of

$$P_e = \frac{2\pi y_{\max}}{v_e} \quad (\text{about } 7.2 \text{ ps for } E=100 \text{ MV/m and } B=5 \text{ T})$$

and drift velocity perpendicular to the electric and magnetic fields equal to the average cycloidal velocity of the electron

$$v_{\text{avg}} = \frac{E}{B} \quad (\text{about } 2 \times 10^7 \text{ m/s for } E=100 \text{ MV/m and } B=5 \text{ T})$$

Because the motion is cycloidal, there is a constant acceleration of the electron of

$$\dot{v}_e = \frac{q_e}{m_e} E \quad (\text{about } 1.8 \times 10^{19} \text{ m/s}^2 \text{ for } E=100 \text{ MV/m and } B=5 \text{ T})$$

Because the electron feels a constant acceleration, there is a constant loss of energy. The dominant frequency of the radiation is the inverse of the period above,

$$f_{\text{dominant}} = \frac{v_e}{2\pi y_{\max}} \quad (\text{about } 14 \text{ GHz for } E=100 \text{ MV/m and } B=5 \text{ T})$$

with a wavelength of about 2 mm.

The energy loss for an accelerated electron is given by Larmor's venerable formula,

$$\begin{aligned} \frac{dW}{dt} &= \frac{2}{3} \frac{q_e^2}{4\pi\epsilon c^3} \dot{v}^2 \\ &= \frac{2}{3} \frac{q_e^2}{4\pi\epsilon c^3} \left( \frac{q_e E}{m_e} \right)^2 \end{aligned}$$

where the second form applies only to the case at hand. Equating this power loss with a rate of change of potential energy, we have the radiation-loss drift velocity of the electrons between the conducting plates,

$$\frac{dW}{dt} = q_e E \frac{dy}{dt} \Rightarrow \frac{dy}{dt} = \frac{q_e^3 E_y}{6\pi\epsilon m_e^2 c^3} \quad (\text{about } 0.1 \text{ mm/s for } E=100 \text{ MV/m and } B=5 \text{ T})$$

This result applies only to electrons starting at rest on the cathode of the transmission line forced into a cycloidal motion by the electric and magnetic fields.

This form of the radiation-loss drift velocity from the cathode to the anode is really the result of hindsight. The original thought process found the energy loss per cycle and equated that to a change in the new starting position (potential energy) of the electron in

the y direction after it had come to a stop. The radiation-loss drift velocity in the direction of the electric field was then found by dividing by the period of the cycloidal motion.

Larmor's form of the power lost by an accelerated particle gives rise to a simple numerical form for the subsequent change in velocity of the particle,

$$\begin{aligned} \frac{dW}{dt} &= \frac{2}{3} \frac{q^2}{4\pi\epsilon c^3} \dot{v}_{\text{total acceleration}}^2 \\ &= \frac{d}{dt} \left( \frac{1}{2} mv^2 \right) \\ &= m v \dot{v}_{\text{acceleration due to radiation losses}} \end{aligned}$$

or, with the vector nature of the loss occurring in the direction of motion,

$$\dot{v}_{\text{acceleration due to radiation losses}} = - \frac{q^2}{6\pi\epsilon c^3} \dot{v}_{\text{total acceleration}} \frac{\vec{v}}{mv^2}$$

A simple code output showing the change in the starting (at-rest) position of the electron is given in Figure D-2.. In this example, the electric and magnetic fields are  $10^8$  V/m and 5 T respectively and the effective radiation-loss drift velocity of the electron has been increased by a factor of  $10^9$  to show a perceptible motion of the electron in the y direction.

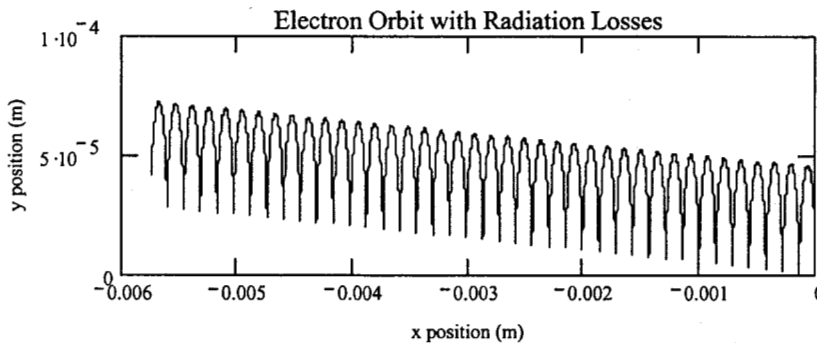


**Figure D-2. Orbit of single electron with radiation losses multiplied by  $10^9$  (motion is right to left for  $E_y = -100$  MV/m and  $B_z = 5$  T)**